Organic Process Research & Development

Article

pubs.acs.org/OPRD

Development and Scale-Up of a Continuous, High-Pressure, Asymmetric Hydrogenation Reaction, Workup, and Isolation

Martin D. Johnson,*[,†] Scott A. May,*[,†] Joel R. Calvin,[†] Jacob Remacle,[†,⊥] James R. Stout,[†,§,∥] William D. Diseroad,[†] Nikolay Zaborenko,[†] Brian D. Haeberle,[†] Wei-Ming Sun,[†] Michael T. Miller,[‡] and John Brennan[†]

[†]Chemical Product Research and Development Eli Lilly and Company, Indianapolis, Indiana 46285, United States

[‡]Analytical Sciences Research and Development, Eli Lilly and Company, Indianapolis, Indiana 46285, United States

[§]D&M Continuous Solutions, LLC, Greenwood, Indiana 46143, United States

ABSTRACT: A fully continuous process including an asymmetric hydrogenation reaction operating at 70 bar hydrogen, aqueous extraction, and crystallization was designed, developed, and demonstrated at pilot scale. This paper highlights safety, quality, and throughput advantages of the continuous reaction and separations unit operations. Production of 144 kg of product was accomplished in laboratory fume hoods and a laboratory hydrogenation bunker over two continuous campaigns. Maximum continuous flow vessel size in the lab hoods was 22 L glassware, and maximum plug flow tube reactor (PFR) size in the bunker was 73 L. The main safety advantages of running the hydrogenation reaction continuous rather than batch were that the flow reactor was smaller for the same throughput and, more importantly, the tubular hydrogenation reactor ran 95% liquid filled at steady state. Therefore, the amount of hydrogen in the reactor at any one time was less than that of batch. A two-stage mixed suspension−mixed product removal (MSMPR) cascade was used for continuous crystallization. Impurity rejection by continuous crystallization was superior to that by batch because scalable residence time and steady-state supersaturation enabled robust and repeatable control of enantiomer rejection in a kinetic regime, although this is a nonstandard approach, debatable as an impurity control strategy. The fully continuous wet-end process running in a laboratory infrastructure achieved the same weekly throughput that would be expected from traditional batch processing in a plant module with 400 L vessels.

INTRODUCTION

Continuous processing has long been recognized as a method for process intensification in the specialty and commodity chemical industry. With the possible exception of select high-volume products, the pharmaceutical industry has lagged behind other industries in the development and application of continuous processes. The synthesis of intermediates and active pharmaceutical ingredients (API) has long relied upon the use of multipurpose batch capacity for development and commercialization. The result of this has been the development of a broad network of batch capacity with process chemists and chemical engineers tasked with developing chemistry amenable to this specific infrastructure, which typically limits operating pressures to less than 10 bar for most plant reaction vessels. There are many examples of specialists in asymmetric hydrogenation building plants with batch reactors capable of 50−100 bar hydrogen pressure, but this high-cost investment is not commonly made in typical multipurpose cGMP pharmaceutical production facilities. This may not be surprising given the long development timelines, high degree of uncertainty in the approval process, and difficulties in predicting the peak volume. In order to install specialized equipment, capital investment would need to be made at risk since the fate of the product in late-phase clinical trials may not be known. The development of new synthetic routes for APIs is therefore not just the "best processes," but rather processes chosen on the basis of available batch capacity and capability. This singular focus on batch capacity restricts the industry from advancing in a number of important areas such as safety, environmental impact, quality by design, process efficiency, and simplest synthetic routes. Recently, a surge of interest in continuous processing from academia and industry has refocused the attention on how the drug discovery, development, and commercialization processes may benefit from continuous processing technology.[1]

We recently reported a rhodium-catalyzed method for chemo- and enantioselective reduction of tetrasubstituted enone **1** to afford ketone **2**, a key intermediate in the synthesis of **LY500307** (Scheme 1).[2] The enantioselective reduction of tetrasubstituted alkenes has long been identified as a significant challenge,[3] and very few examples of highly catalytic processes are known at any scale.[4] The conditions identified for the reduction of **1** required hydrogen pressure up to 70 bar in order to obtain commercially viable substrate-to-catalyst loading (S/C). This high-pressure requirement posed a serious development concern, as equipment to perform this chemistry was not available in our manufacturing area, and significant capital investment would have been required to install this step. In addition to the pressure requirement, the chiral purity of **2** had to be improved from ∼94% ee in the crude reaction product to >99% in the isolated product. The challenge associated with this unit operation was that **2** has an unfavorable eutectic point,

Special Issue: Continuous Processes 2012

Received: December 9, 2011
Published: April 27, 2012

   dx.doi.org/10.1021/op200362h | *Org. Process Res. Dev.* 2012, 16, 1017−1038

Scheme 1. Asymmetric reduction of enone 1 and the synthesis of LY500307

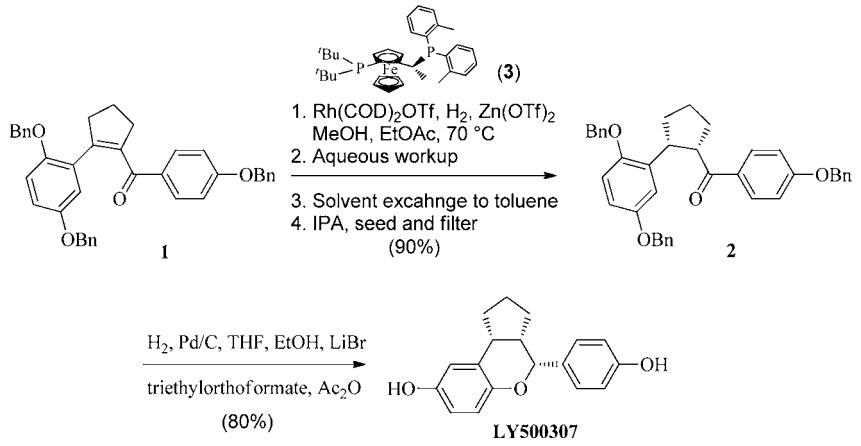

leading to an upgrade only by kinetically controlled crystallization. We report herein the development of a fully continuous wet-end process, including reaction, workup, and crystallization, for the synthesis of **2**. We highlight the use of high-pressure tubular or pipe reactors as practical, safer, and economical alternatives to standard batch hydrogenation infrastructure for homogeneous catalytic reactions. In addition we also report continuous extraction, automated repeating semibatch solvent exchange distillation with strip to dryness, and a scalable kinetically controlled continuous crystallization in MSMPR crystallizers that allows for reliable upgrade of enantiopurity in the kinetic regime. Safety, quality, and throughput advantages of the continuous reaction and separations unit operations will be described through the production of 144 kg (86% isolated yield) of **2** in laboratory fume hoods and a laboratory hydrogenation bunker.

RESULTS AND DISCUSSION

Batch Reaction Parameters. The preferred synthetic route toward **LY500307** involved a high-pressure asymmetric hydrogenation of ketone **1** to provide penultimate intermediate **2** (Scheme 1). During development, a remarkable synergistic effect was found wherein catalytic zinc triflate dramatically enhanced catalyst turnover frequency, as shown in entries 1 and 2 of Table 1. This discovery allowed the catalyst loading to

Table 1. Key reaction parameters for the reduction of 1

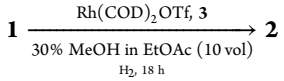

entry	$Zn(OTf)_2$ (equiv)	S/C	T (°C)	conversion (%)	H_2 (bar)	ee (%)
1	0	1000	50	2	28	–
2	0.1	1000	50	100	28	95.8
3	0.1	2000	50	91	28	96.0
4	0.1	4000	50	41	28	96.2
5	0.1	3000	95	100	28	94.2
6	0.1	4000	70	100	70	94.0

approach levels that would be practical for commercial development. The reaction rate was further enhanced by both temperature (entry 5) and pressure (entry 6) with minimal effect on enantioselectivity.

Running optimized conditions (S/C 4000, 0.1 equiv $Zn(OTf)_2$, 70 bar hydrogen, 30% MeOH/EtOAc, 70 °C, 18 h) at 10 g scale in a batch autoclave afforded **2** in 90% yield (>99.9% ee) after workup and crystallization from toluene and isopropyl alcohol. Typical related substances during the reaction were enantiomer **4**, phenolic ester **5**, and epimerization product **6**. Phenolic ester **5** was introduced as an impurity in

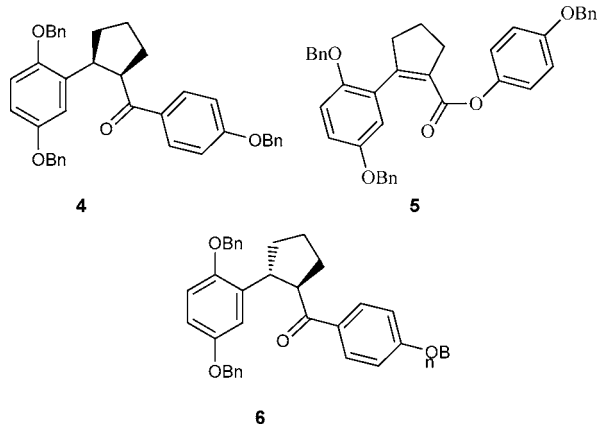

the starting material and did not react under the hydrogenation conditions.[5] Impurity **6** was found to form at elevated temperatures in the presence of strong acid over time.

While the results from the reaction development were encouraging, the prospect of commercializing a high-pressure asymmetric hydrogenation was of serious safety and capital cost concern. The batch infrastructure to perform such a reaction was not available to us in our manufacturing area. The possibility of investing in additional specialized batch capacity was unappealing and untenable because the fate of the API as a commercial product had not yet been firmly established. Without a clear return on investment, a decision to invest in a large-batch high-pressure autoclave would represent a significant financial risk. Furthermore, even if **LY500307** became a commercial product, a complete understanding of peak volume might not be clear until much later in the product lifecycle, adding uncertainty to the size of the investment in infrastructure. For these reasons, we chose to explore continuous processing with portable equipment as a practical, safer, and more flexible alternative to installing additional specialized batch capacity for high-pressure hydrogenation.

Continuous Hydrogenation Reactor Design. Continuous flow hydrogenation is not a new concept. Several literature examples that have been demonstrated, at least at research scale, are listed in Table 2. This table also illustrates the wide

dx.doi.org/10.1021/op200362h | Org. Process Res. Dev. 2012, 16, 1017–1038

Table 2. Comparison of select continuous reactor types used in asymmetric hydrogenation

reactor type	τ and P	catalyst	substrate	ref
micro channel mixer followed by tube reactor	τ = 2−12 min P = 3−11 bar	[Rh(*S*,*S*-BDPPTS)] (S/C 20−70)	alkene (*Z*)-α-acetamidocinnamate	6
helicoidal single channel falling film micro reactor	τ = 3−22 min P = 1 bar	$[Rh(COD)_2]BF_4$ ligand?	alkene (*Z*)-α-acetamidocinnamate	7
Packed bed reactor in $scCO_2$	τ = not reported P = 60−120 bar	immobilized [Rh(*S*,*S*-Skewphos) (nbd)](BF_4) on alumina	alkene(dimethyl itaconate)	8
packed bed reactor	τ = not reported P = 10−200 bar	chirally modified 5% Pt/alumina	ketone(ethyl pyruvate)	9
coiled tube reactor	τ = 6−9 h P = 69 bar	$[Rh(COD)_2]BF_4$/Josiphos-505 (S/C 2000)	alkene(enone)**1**	this report

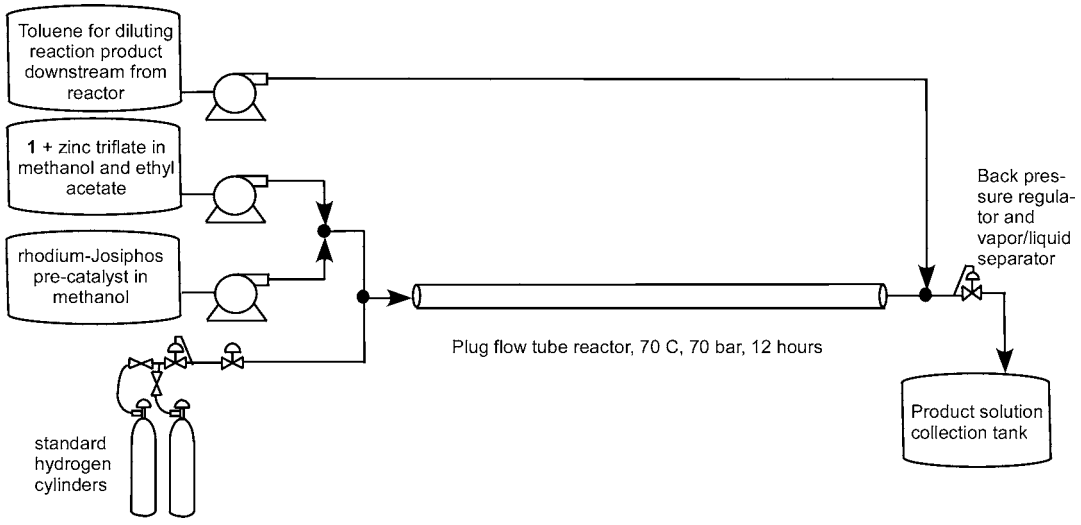

Figure 1. Continuous reactor configuration used for 1.46 and 73 L PFRs.

variety of continuous reactor types and catalysts. Furthermore, operating conditions used by these researchers covered a wide range of catalyst types, hydrogen pressures (1−200 bar), reaction temperatures (20−100 °C), substrates, and dissolved substrate concentrations (0.01−2.5 M). Table 2 shows examples of enantioselective hydrogenation with fixed, solid, bound catalysts and with dissolved catalyst. In comparison to the reactor types shown in Table 2, the type of continuous reactor used in this study (coiled tubes with standard piping "T"s) has relatively low complexity. Also, comparing our approach to most of the others, we used relatively higher S/C which is important for economical scale-up, longer mean liquid residence time in the flow reactor (τ) which is required for maximizing S/C, and longer steady-state time durations which is important for demonstrating process reliability, robustness, and quality.

One of the potential problems with packed bed or otherwise sequestered catalyst for continuous hydrogenation reactions in a cGMP environment is that catalyst activity can change over time. Therefore, it is possible that not every 24- or 48-h "batch" will be the same in terms of yield or impurity profile, because the catalyst is a fixed part of the reactor. Any fixed catalyst may degrade over time and require a detailed understanding of degradation kinetics so the catalyst could be replaced after a certain amount of time. The choice of stable, homogeneous catalysts makes them better suited for continuous flow hydrogenation reaction in tubular reactors.

Reactor technology choice in this work was a concurrent plug flow tube reactor (PFR) as shown in Figure 1. Both research-scale (as small as 10 mL) and pilot-scale (70 L) systems were designed and constructed. Two high-pressure pumps deliver solutions of starting enone **1** and zinc triflate from one pump and a solution of precatalyst in the second pump. The two feeds combine at a specified ratio in a mixing "T" and flow through tubing of sufficient length and inside diameter so that they are well mixed. Hydrogen gas combines continuously in a second mixing "T" at the PFR inlet. This combined liquid and vapor mixture then enters the PFR and flows through concurrently. The reactor is designed for full conversion in a single pass (with no recycle or pump-around) through a series of single tubes (with no parallel flow channels). Toluene continuously pumps into a mixing "T" at the exit of the PFR to ensure product solubility at room temperature and to facilitate extractive workup downstream. The diluted product solution exits the reactor, passes through a back-pressure regulating system, separates from the excess hydrogen, and collects in a product solution tank. Sampling of the reaction product solution both manually and in automated fashion is done as the crude product stream moves to the product tank. The manual and automated sampling systems were engineered so that liquid is depressurized to 0 bar and inerted with nitrogen before collection to vials or analyzed by online UPLC (Waters PATROL).

Preparation of the starting material feed solution batches was done in stirred flasks inside a laboratory hood. Starting material solutions were transferred to stainless steel surge tanks that feed the PFR. Surge tanks were paired so that one may be filled while the other supplies the PFR. The feed solution with **1** and zinc triflate in methanol/ethyl acetate was degassed by sparging with nitrogen in the feed tank. The rhodium−Josiphos precatalyst is highly oxygen-sensitive; therefore, it was important to properly inert the reaction solvents and

equipment prior to introducing the catalyst to the system. The air-sensitive precatalyst feed solution was prepared in a glovebox and transferred directly to the offline high-pressure syringe pump. Extreme care was taken to keep the catalyst feed solution inerted and under positive nitrogen pressure at all times so that it would not be contaminated with air after removing the pressure bottle from the glovebox. Manually operated tandem high-pressure syringe pumps were used to ensure uninterrupted catalyst/ligand solution flow to the reactor.

RESULTS

The reaction was run in a 1.46 L PFR before running at pilot scale. The reactor was made of 316 L stainless steel tubing with outside diameter (o.d.) = 3.18 mm, inside diameter (d) = 2.01 mm, and length (L) = 457 m, coiled and placed inside a 20 L constant temperature oil bath. Vapor and liquid flow was segmented in tubing of this diameter, such that average vapor velocity equals average liquid velocity at each point along the length of the PFR. In one continuous 114 h run, a total of 456 g **2** was produced. Effects of S/C, molar equivalents of hydrogen, and τ were studied. Vapor-to-liquid volumetric flow ratio was carefully controlled in order to achieve the desired τ in the tube as represented in Table 3.

Table 3. Reaction performance in 1.46-L PFR

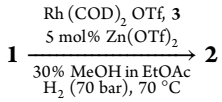

entry	S/C	conversion (%)	H_2 (mol equiv)	τ (h)
1	1000	99.9	13	12
2	2000	99.6	13	6
3	3000	99.4	13	12
4	4000	93.8	13	12
5	2000	99.6	3.5	12
6	2000	99.4	3.5	6
7	3000	97.2	3.5	12

As shown in entries 1−3 of Table 3, full conversion was observed at S/C loadings of up to 3000 within a τ = 12 h. When S/C was increased to 4000 (entry 4) full conversion was not reached at τ = 12 h. Entries 2 and 6 showed that τ = 6 h was sufficient for 99.4% conversion at S/C = 2000 for a wide range of hydrogen flow rates. The observed enantiomeric excess did not appreciably change (94−95% ee) nor did the impurity profile across all of the conditions described. Entries 3 and 7 in Table 3 indicate that conversion was higher when more excess hydrogen was used, all else remaining constant. Vapor−liquid mass transfer is expected to be enhanced at higher gas/liquid ratio. The two-phase flow was segmented into alternating vapor bubbles and liquid slugs traveling along the length of this stainless steel tube with d = 2 mm. Mixing occurs in each liquid slug through recirculatory motion.[10] The average linear velocity of liquid slugs along the 457 m tube length was controlled to be the about same in both cases, entries 3 and 7, but the average liquid slug length between gas bubbles was shorter, and the slugs were more frequent when more excess hydrogen was used. This increased the total vapor/liquid interfacial surface area in the 2 mm diameter reactor. In addition, hydrogen gas diffuses into the liquid film layer on the walls surrounding each gas bubble. This liquid film can be on the order of 1 μm thick and depends on relative magnitude of viscous to surface tension forces and surface properties.[11]

The plug flow tube hydrogenation reactor (Figure 2) used for pilot-scale reaction was 73 L. Material of construction was

Figure 2. Pilot-scale 73 L coiled-tube reactor.

316 L stainless steel tubing with o.d. = 19.1 mm, d = 16.5 mm, and L = 340 m. The tubing was formed into eight concentric cylindrical coils 0.53 m tall and ranging from 0.36 to 0.80 m diameter as pictured. Vapor and liquid flow concurrently through each of the eight coils in series in the uphill direction starting with the outside coil. These individual coils are linked by down-jumper tubes constructed from 316 L stainless steel tubing with o.d. = 6.35 mm and d = 4.57 mm. The reactor was designed this way to maintain maximum volume in the uphill flow direction (>98% of the total reactor volume) which allowed the reactor to run almost completely liquid filled in the forward direction. This also made it possible to almost completely empty solvent from the reactor by pushing with nitrogen in the reverse direction at the end of the run. The overall height and diameter of the cylindrical coiled tubing assembly was designed to fit inside an existing 0.91 m diameter single-plate filter, which was jacketed and used as a constant temperature bath for the reaction. A flow cart with automated valves and pressure transmitters connecting the reactor, the pumps, and the receivers was constructed as a mobile unit.[12] The flow cart was operated by the DeltaV digital automation system to control reactor pressure and vapor/liquid flow ratio, and to depressurize the product stream from 69 to 0 bar gauge at the reactor exit and dilute the off-gas with nitrogen before venting.

Two campaigns were performed using the 73 L coiled-tube reactor. The first campaign ran for 282 h total cumulative reagent feed time, and the second 56 h reagent feed time. Table 4 summarizes the different steady-state conditions and resulting conversion and enantiomeric excesses throughout both campaigns. After each step-change in process parameters, time to steady state was in the range 12−20 h, as indirectly conveyed in Table 4.

dx.doi.org/10.1021/op200362h | Org. Process Res. Dev. 2012, 16, 1017−1038

Table 4. Reaction parameters in the two continuous-flow hydrogenation campaigns

campaign	flow time (h)	τ (h)	T (°C)	S/C	conversion (%)	ee (%)
1	14–102	12	70	1992	>99.8	94.4
	116–289	13	70		>99.8	94.4
2	12–14.3	11.8	90	1880	>99.8	93.7
	32–48	12	70		>99.8	94.0
	52–65	9.9	70		>99.8	94.9

A startup transition was observed where the reaction was dynamic prior to reaching a steady state because the PFR started liquid-filled with solvent only. This can be seen in a and b of Figure 3 as product concentration rises from t = 0 h to a steady-state value around t = 12 h in both cases, which is about 1 mean residence time. Likewise, at the end of the reaction, product concentration dropped when product was pushed out of the reactor by solvent. In campaign 1 (Figure 3a), the gas/liquid volumetric flow ratio at the outlet before depressurization was initially set to 0.58 (9 equiv of hydrogen) at the beginning, then gradually reduced to 0.1 (1.3 equiv of hydrogen) by the end of the 282 h run. At the latter level, the liquid fill fraction of the reactor was ~93–95%. Vapor travels through the inclined PFR tubes (d = 16 mm) at a higher average velocity than liquid. In addition to density differences between gas and liquid phases, this is promoted by oscillatory flow resulting from the deliberate pressure pulses from the expansion chambers in series, which are used to depressurize liquid and vapor flowing out the end of the reactor.

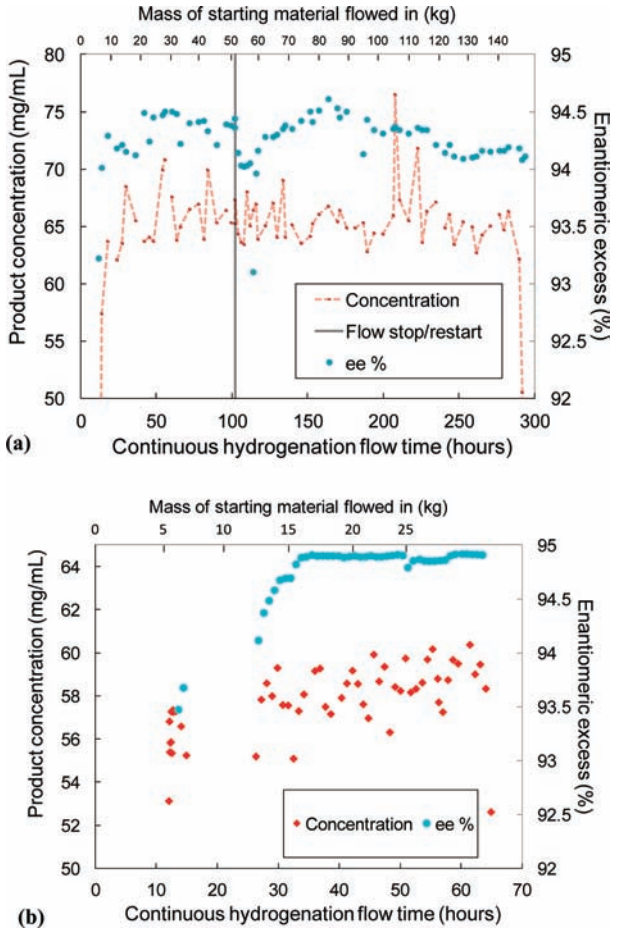

Figure 3. Product concentration and ee % vs time for (a) campaign 1 (b) campaign 2.

Figure 3b represents the second campaign, and similar startup and pushout transitions can be observed. Concentration and ee analytical data at steady state in Figure 3b show less scatter than in the first campaign (Figure 3a), as shown by the standard deviations in Table 5. The narrower concentration distribution in the second campaign section was due to the use of an automated online UPLC for sampling and analysis, which greatly reduced inconsistency in sample preparation. This was especially evident in the ee data. The PAT was especially helpful in that it reduced the overall people time and data turnaround time by at least 10× while increasing the amount and consistency of the data.

Table 5. Average product concentrations and ee % with standard deviations

campaign	flow time (h)	[**2**] average (mg/mL)	[**2**] standard deviation (%)	average ee (%)	ee standard deviation (%)
1	116–289	65.59	3.75	94.29	0.155
2	34–48	58.28	1.76	94.89	0.019

After the first 102 h of flow in campaign 1, all gas and liquid flows were stopped (vertical line in Figure 3a), and the reactor inlet and outlet valves were closed for 65.4 h for an intentional weekend shutdown. The graph does not reflect the time of this shutdown. The reactor was held at 70 °C under hydrogen (70 bar) throughout the hold. This did not affect the product concentration; however, an impurity did increase during the 65-h hold time (Figure 4). The high *trans* impurity (**6**) pushed out for the first 1.1 volume turnovers after flow resumed. Epimerization product **6** formed in this case as a result of triflic acid, which was a known low-level contaminant in the lot of zinc triflate used. In campaign 2, improvements to the process allowed for a reduction in the quantity of zinc triflate from 0.10 to 0.05 equiv, and tighter control over zinc triflate quality led to very low (<0.10%) levels of **6** at steady state.

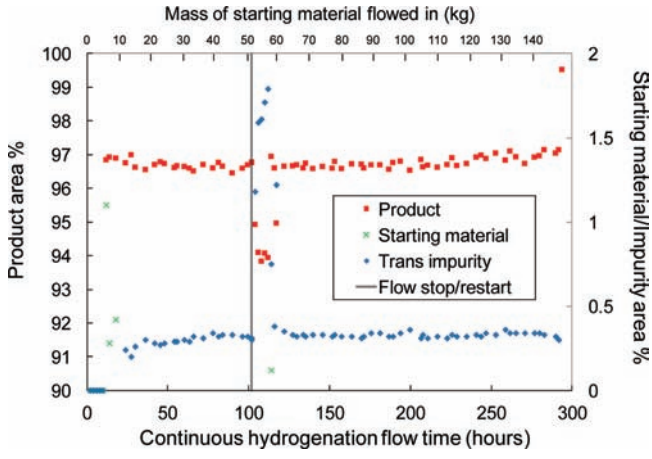

Figure 4. HPLC area % of **2**, **1**, and *trans* impurity **6** in campaign 1.

Consider PFR vs batch in terms of safety and throughput. For the same throughput, a batch reactor would need to be at least twice as large as the PFR, assuming that it can be reacting half the time, while the other half of the time is for filling, purging/inerting, pressurizing, emptying, and rinsing. In

dx.doi.org/10.1021/op200362h | *Org. Process Res. Dev.* 2012, 16, 1017–1038

contrast, the PFR is reacting 100% of the time. In the campaign reported in this paper, the PFR was 93−95% liquid filled at steady state. Furthermore, we have run the same type of reaction in PFRs with vertical pipes in series that operate >98% liquid filled overall at steady state. Assuming that the batch reactor operates 80% liquid filled, and that the batch reactor volume is twice the PFR, headspace volume in the batch reactor would be 20 times more than headspace volume in the PFR. Less hydrogen in the reactor at any one time is the main safety advantage of the continuous reaction. In addition, instantaneous hydrogen feed rate from the supply cylinders (or generator) is much less for the PFR because the hydrogen is slowly metered at steady state, as opposed to batch where the headspace is purged and then pressured up to 70 bar with hydrogen over a short period of time. Finally, lower capital expenditure represents an advantage in favor of continuous high pressure hydrogenations for manufacturing sites that do not already have existing batch equipment capacity for 70 bar hydrogenations.

It is important to note that most of the design and development work for this continuous process was done through research-scale batch experiments. The continuous flow experiments at research- and pilot scale served to verify that heat- and mass transfer rates were sufficient in the selected equipment types so that results matched expectations from the batch experiments. In other words, to design and develop an homogeneously catalyzed asymmetric hydrogenation process, very little of the research-scale design and development work needed to be done in continuous processing equipment.

Reactor Characterization. In an ideal PFR, the time to achieve a given percent conversion of reagents is the same as in an ideal batch reactor. This can be easily shown mathematically.[13] Design equations for time to reach a given percent conversion in batch and plug flow reactors can be derived from the point form of the continuity equation, which describes the total material balance of component i around the differential volume.

Equation 1. Point form of the material balance equation for a reactor:

$$-\nabla \cdot N_i + r_i = \frac{\partial C_i}{\partial t} \tag{1}$$

$-\nabla \cdot N_i$ = mass flow of component i into and out of a differential volume inside the reactor.

r_i = reaction rate of component i within the differential volume

$\partial C_i/\partial t$ accumulation rate of component i within the differential volume

For a batch reactor, the first term in eq 1 equals zero because there is no flow in or out. The equation is then integrated over all differential volumes in the reactor because we assume that the vessel is perfectly mixed, and therefore concentration is uniform throughout (eq 2). For an ideal PFR, on the other hand, the last term in eq 1 equals zero because there is no accumulation at steady state. The equation is then integrated over the entire distance of the reactor in the axial direction because there is no change in concentration in the radial direction (eq 3). However, the mathematical forms of the integrals to calculate reaction conversion vs time are identical.

Equation 2 is the continuity equation integrated for an ideal batch reactor:

$$t = \int_0^t \mathrm{d}t = \int_{C_0}^{C_t} \frac{\mathrm{d}C}{r} \tag{2}$$

where

t = time,

r = reaction rate within the differential volume,

C_0 = concentration at time zero, and

C_t = concentration at time t.

Equation 3 is the continuity equation integrated for an ideal plug flow reactor:

$$\int_0^L \frac{1}{\nu_x}\mathrm{d}x = \frac{L}{\nu_x} = \bar{t} = \int_{C_{\mathrm{IN}}}^{C_{\mathrm{OUT}}} \frac{\mathrm{d}C}{r} \tag{3}$$

where

ν_x = flow velocity in the axial direction along the plug flow tube,

L = length of ideal plug flow tube reactor, and

$\bar{t}$ = time inside the ideal plug flow tube reactor.

Real reactors are not ideal because mixing in the radial direction is not 100% and mixing in the axial direction is not zero. Dispersion in the axial direction causes some fluid elements to travel through the reactor faster than others. Axial dispersion must be quantified so that it can be used in the nonideal plug flow with dispersion reactor model (PFDR) to calculate τ to a given percent conversion in a real tubular reactor. If we know axial dispersion and reaction kinetics for a positive order reaction, then this information can be used to quantify how much more time would be required for a given percent conversion in a PFDR compared to that in an ideal PFR or batch reactor. Fractional conversion of reactant A as it passes through a PFDR is governed by axial dispersion, bulk flow, reaction rate, and reaction order, as shown in the following dimensionless form of the material balance equation for component A (eq 4).

Equation 4 is the material balance equation for a plug flow with dispersion reactor.

$$\frac{D}{uL}\frac{d^2X_A}{\mathrm{d}z^2} - \frac{\mathrm{d}X_A}{\mathrm{d}z} + k\tau C_{A0}^{n-1}(1 - X_A)^n = 0 \tag{4}$$

where

X_A = fractional conversion,

C_{A_0}= initial concentration,

z = fraction of total reactor length (l/L),

k = reaction rate constant, and

n = reaction order

Maintaining similar residence time distribution (RTD) with scale-up/-down is essential so that conversion vs τ remains constant. This means that deviations from plug flow in the tube should be similar with scale-up/-down, characterized by axial dispersion.

In a separate contribution[14] we provide a detailed description of axial dispersion in terms of vessel dispersion number (D/uL where D is the Taylor longitudinal dispersion coefficient that incorporates the effect of both diffusion and convection,u is average flow velocity, and L is vessel length) and methods for quantifying D/uL by experimentally measuring "F-curves" and numerically modeling the data, following textbook methods. That report[14] explains the relationship between D/uL, tube length to internal diameter ratio (L/d), and dispersion intensity (D/ud), which is a function of Reynolds number (Re) and Schmidt number (Sc). It provides data and explanations for why higher L/d results in lower D/uL for laminar flow tubes,

dx.doi.org/10.1021/op200362h | Org. Process Res. Dev. 2012, 16, 1017−1038

and why D/uL is lower at slower flow rates for the smaller diameter tubes (example d = 2 mm), but it is higher at slower flow rates for the larger diameter tubes (for example d = 16 mm) in the laminar flow regime. It describes calculation of reaction time for conversion of reagents as a function of reaction rate and axial dispersion.

Axial dispersion increases required reaction time for a given fractional conversion. The higher the value of D/uL, the greater impact axial dispersion will have on reaction time. For example, for an elementary first-order reaction, if D/uL = 0.001, then τ to reach 99.9% conversion of reagent is only about 1% longer than in an ideal PFR. However, τ is 63% longer than ideal PFR to reach 99.9% conversion if D/uL = 0.1. The axial dispersion number was determined for the 1.46 L tube reactor at four different flow conditions and for the 73 L tube reactor at three different flow conditions, listed in Table 6. The F-curves measured for each of these solvent flow tests are respectively shown in Figures 5 and 6.

Table 6. Characterization of axial dispersion number for the 1.46- and 73 L tube reactors with solvent and nitrogen flow at low pressure

entry	V (L)	τ (min)	vapor/liquid flow ratio	Re	D/uL
1	1.46	867	0.25	ND	0.0000054
2	1.46	719	0	36	0.0000648
3	1.46	91	0	285	0.0002200
4	1.46	9	0	2880	0.0001400
5	73	858	0.25	ND	0.00032
6	73	708	0	213	0.00247
7	73	50	0	3010	0.00049

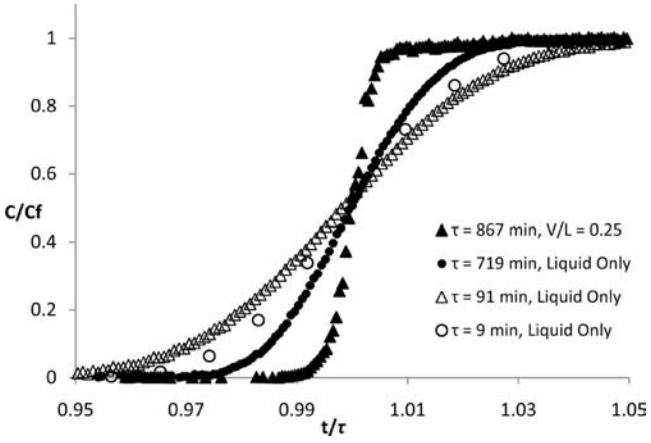

Figure 5. Axial dispersion tests with solvents, at four different flow conditions, for the 1.46 L PFR.

For each solvent-only axial dispersion experiment, the F-curve was obtained by making a step change from 100% THF to a 60%/40% (v/v) THF/toluene mixture flowing into the tube, and monitoring the concentration of toluene in the reactor effluent with an online Raman probe. Nitrogen was used for the experiments with two-phase gas/liquid flow, which mixed with the solvents at the tube reactor inlet. In the figures, C/C_f is the normalized toluene concentration relative to the new steady-state concentration after the step change, and t/τ is normalized time, where t/τ = 1 represents one mean volume turnover.

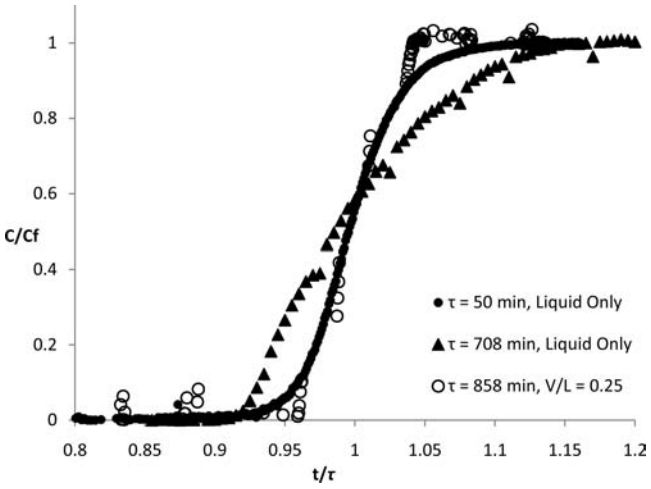

Figure 6. Axial dispersion tests with solvents, at three different flow conditions, for the 73 L PFR.

Entry 1 in Table 6 was most representative of the hydrogenation reactions in the 1.46 L tube reactor, and entry 5 was most representative of flow during the hydrogenation reactions in the 73 L tube reactor. Dispersion numbers in these two flow tests were D/uL = 0.0000054 and D/uL = 0.00032, respectively. These are both extremely low axial dispersion numbers and therefore they represent nearly ideal plug flow behavior. The axial dispersion number for the 1.46 L tube reactor in particular is remarkably low. In both the 1.46 L and the 73 L tubes, D/uL was lower for two-phase gas/liquid flow than for flow with liquid only in the laminar regime. In other words, the tubes were closer to ideal plug flow with gas bubbles present than without. Considering the 2 mm diameter reactor with alternating liquid slugs and vapor bubbles which approximately fill the cross section, the result is similar to published observations that micro reactors with interior meandering channel dimensions 0.400 mm wide and 0.115 mm deep also have lower axial dispersion for segmented gas–liquid flow vs single-phase liquid flow, as evidenced by 5 times to 8 times lower variance of the RTD curve.[15] Vapor and liquid are separated into discrete slugs in both cases. In the 73 L tube reactor, however, flow is not segmented in the same way because not all vapor bubbles occupy the entire tube cross section and gas travels through the up-flow tubes faster than liquid on average. However, the gas bubbles still serve to increase mixing in the radial direction relative to the longitudinal mixing of parabolic velocity profiles in the laminar flow tube, as evidenced by lower axial dispersion with gas flow than without. It is worth mentioning that when we scale up further to larger diameter vertical pipes in series the gas bubbles can increase D/uL compared to liquid only.

Looking at the liquid-only flow rate tests in Table 6, an interesting contrast can be seen. In the 1.46 L tube with d = 2.01 mm, axial dispersion is less at slower flow rates. However, the opposite is true for the 73 L tube reactor with d = 16.5 mm, where axial dispersion is less for the faster flow rates. This is expected because mixing in the radial direction is dominated by diffusion in the 1.46 L reactor (d = 2 mm) at low Reynolds numbers (Re = 36 at τ = 719 min, and Re = 285 at τ = 91 min), while mixing in the radial direction is dominated by turbulence in the 73 L tube reactor (d = 16.5 mm) at high Reynolds numbers (Re = 3010 at τ = 50 min). In fact, when the flow rate through the 1.46 L tube reactor is high enough to achieve

dx.doi.org/10.1021/op200362h | Org. Process Res. Dev. 2012, 16, 1017–1038

turbulence (Re = 2880 at τ = 9 min), axial dispersion does decrease relative to the slower flow rate (Re = 285 at τ = 91 min), as D/uL decreases from 0.00022 to 0.00014. These trends of D/uL for liquid flow in tubes agree with correlations found in the Levenspiel 1962 text based on Re, Schmidt number (Sc), and geometric factor (L/d), as seen in Figure 7

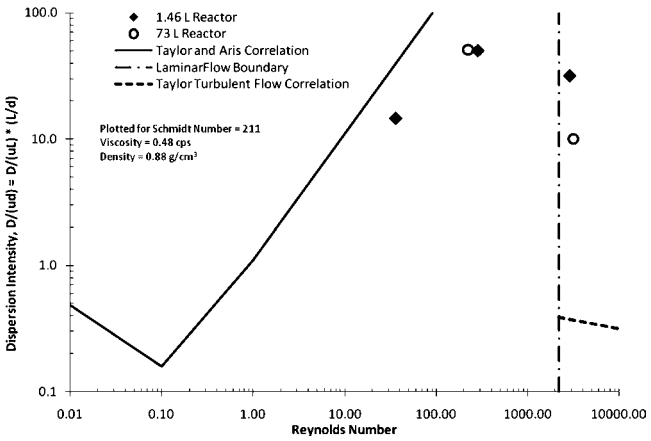

Figure 7. Dispersion intensity, experimental vs Taylor and Aris correlations.

However, this present work applies the correlations to higher L/d ratio and τ than previous researchers. The data does not match the theoretical prediction exactly, but the trend holds valid that, for a given L/d and Sc, D/uL increases as Re increases in the laminar regime, then it decreases as Re continues to increase into the turbulent regime. Furthermore, in any flow regime for a given D/ud, Re, and Sc, one way to decrease D/uL is to decrease d/L.

While all of the above are interesting and important characterizations, for practical purposes axial dispersion is low in all cases, and both reactors can be modeled as ideal PFRs with negligible error in conversion vs time predictions.

The 73 L tube reactor (Figure 2) used for the pilot-scale reaction was also characterized for axial dispersion during startup transition from solvent-only to hydrogenation reaction with product compound **2**. Figure 8 shows data from reaction startup during campaigns 1 and 2. In addition, it shows

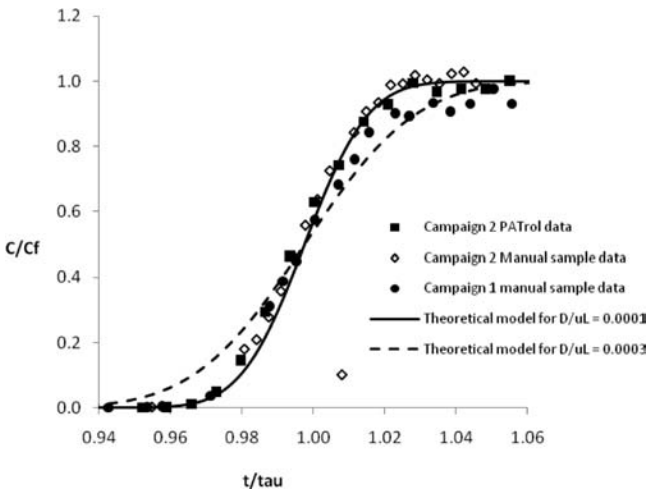

Figure 8. F-curves measured during startup transitions from solvent-only, compared to theoretical F-curves.

concentration vs t/τ data for campaign 2 measured by two different methods: first, by taking samples manually and analyzing offline by HPLC and, second, by automated online PATROL UPLC. In Figure 8, C/C_f is the normalized concentration of **2** relative to the steady-state concentration of 7.0 wt %, and t/τ is normalized time where t/τ = 1 represents one volume turnover at τ = 12 h. Theoretical dispersion model fits with D/uL = 0.0001 and D/uL = 0.0003 are included. The fact that axial dispersion was about the same for both campaigns shows repeatability. Comparison to theoretical curves with D/uL = 0.0001 and 0.0003 proves that axial dispersion was indeed very low in this reactor. Furthermore, D/uL = 0.00032 determined for the solvent-only testing at low pressures with the same volumetric gas/liquid flow ratio matched very well with axial dispersion under the actual hydrogenation reaction conditions. The end result is that modeling the reactors as ideal PFRs will introduce less than 1% error compared to modeling conversion vs time in PFDRs, which is why we call the tube reactor a PFR for practical purposes.

Liquid–Liquid Extraction. Downstream from the hydrogenation reaction, the next continuous unit operation was liquid–liquid extraction, primarily to remove zinc salts with dilute HCl, neutralize, and wash the ionic species. A continuous-flow cross-current three-stage mixer–settler system was used for this purpose (Figure 9).[16] All vessels were glass

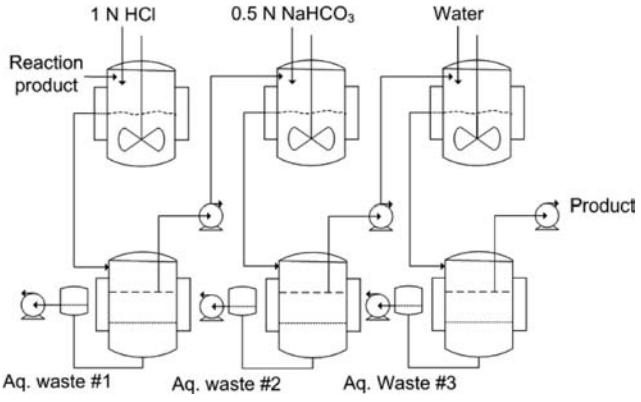

Figure 9. Three-stage cross-current mixer–settler liquid–liquid extraction setup.

22-L round-bottom flasks operating at atmospheric pressure and room temperature. The reaction product solution flowed continuously through the three-stage mixer–settler. HCl (1 N) was pumped into mixer 1, sodium bicarbonate (0.5 N) was pumped into mixer 2, and deionized water was pumped into mixer 3. The two-phase liquid/liquid mixture from each mixer gravity overflowed to the corresponding settler below, and both liquid phases from each settler were continuously pumped out. Pressurized feed tanks, coriolis mass flow meters, and automated control valves were used to control flow rates of all four feeds, and two three-channel peristaltic pumps were used to transfer fluids out of the settlers. The settlers served as gravity decanters, such that the height of the raised aqueous leg flowing from the bottom of the setter and the density ratio controlled the liquid–liquid interface height in the settler. The gravity overflow height of the aqueous phase is located at an elevation between that of the top of the organic layer and liquid–liquid interface in the settler. Increasing or decreasing the aqueous overflow height increases or decreases the liquid–

dx.doi.org/10.1021/op200362h | Org. Process Res. Dev. 2012, 16, 1017–1038

liquid interface height in the settler. Because the organic streams were removed only from the very top of the layer and the aqueous stream was removed only from the very bottom of each settler, only cleanly separated liquid layers furthest from the L/L interface were removed, thus maintaining high quality of separation.

In small scale, τ = 15 min in the mixers and in each settler phase were sufficient to achieve close to 100% stage efficiency. However, for the full scale, τ was selected only to keep pace with the output of the hydrogenation reaction. Thus, τ in the mixers (kept half-full at ~11 L) was 60–90 min, and τ in the settler phases was 90–96 min. At these organic feed stream flow rates, a throughput of 12 kg/day of product was demonstrated, with >99% product recovery. The levels of zinc were reduced from 450 ± 15 μg/mL to <0.5 μg/mL, nearly all of it removed in the first stage by hydrochloric acid (Table 7).

Table 7. Summary of metal removal during continuous three-stage liquid–liquid extraction

campaign	condition[a]	zinc in feed (μg/mL)	zinc in output (μg/mL)	rhodium in feed (μg/mL)	rhodium in output (μg/mL)
1	steady state	419	<0.5	3.5	4.6
	equilibrium	419	<0.5	3.5	5.2
	steady state	419	<0.5	3.5	4.5
	equilibrium	419	0.56	3.5	4.9
2	steady state	ND	0.23	3.7[b]	4.5

[a]"Steady state" indicates samples taken during regular flow operation, while equilibrium refers to samples taken following a 63 h batch-like equilibrium. [b]Rhodium values calculated on the basis of hydrogenation feed composition. Zinc values not measured in Campaign 2, but expected to be about half of the values from campaign 1. Maximum zinc concentration calculated to be 360 μg/mL for campaign 2 and 610 μg/mL in campaign 1 based on reaction feeds, which was slightly higher than measured.

During the first section of the campaign, multiple samples from each of the phases (two per mixer and two per settler) were taken both during steady-state flow operation and following weekend-long pauses in processing, allowing >60 h to reach equilibrium partitioning. Each of these samples was analyzed for metal content (Table 7). Data show that the continuous mixer–settlers ran with nearly 100% stage efficiency with respect to zinc partitioning. Total material balance and in situ mass balance of **2** were both calculated to be within 98–100% for both campaigns 1 and 2.

Rh levels were also monitored in the samples, which was not partitioned into the aqueous phase. The Rh metal was subsequently rejected into the filtrate during crystallization. The crystallization reduced Rh content from about 100 to about 20 ppm (μg Rh/g **2**).

The longest continuous extraction run with no stops was 96 h. The unit operation was shut down at least every weekend, and in the second campaign, every evening (Table 8). At these points, all pumps and agitators were powered off, and the mixtures were allowed to sit in their respective vessels at normal operating levels. The following morning, mixer agitators and pumps were restarted. No transition waste or yield loss was incurred in the stop/restarts. During the second campaign period, only one person did all of the setup and operation of continuous extraction by himself, including startup and shutdown transitions, stopping the flows every night. One of the reasons why mixer–settlers were selected for extraction was that they are easy to stop and restart with no transition waste, and they are easy to operate with very little manual or automated control required.

Table 8. Liquid–liquid extraction continuous-flow campaign summary

campaign	section	flow time (h)[a]	mass **2** (kg)	# of start/stops
1	A	282	143.3	3
	B1	batch	0.34	NA
2	B2	8.7	6.2	3
	C1	32.4	15.5	4
	C2	12.3	4.3	2

[a]Cumulative flow time for each campaign section, not counting down-time during nights and weekends shutdowns.

Multiple advantages of continuous-flow liquid–liquid extraction were demonstrated. The setup consisted of simple, inexpensive, cleanable, and portable equipment, with the three mixer–settlers and all pumps contained in a single lab-scale fume hood. Stainless steel and Hastelloy C276 feed tanks and receiver tanks, 40–80 L each, were outside the lab hood. All phase separation with the exception of final phase splits at shutdown occurred by withdrawal from the cleanest sites in the settlers, furthest removed from the liquid–liquid interface. Continuous mixer-settlers also provided the ability to collect the insoluble material that accumulated at the liquid–liquid interfaces over time, which was high in zinc content. Finally, it gave the opportunity to flow through coalescing screens at the outlet from each mixer which resulted in cleaner phase separations.

Solvent Exchange Distillation. The solvent composition after the extractive work up contained <1% methanol, 46% toluene and 54% ethyl acetate. However, the crystallization of **2** required toluene as the primary solvent with the addition of isopropanol as antisolvent. Therefore solvent exchange from toluene/ethyl acetate to toluene alone was required. Automated repeating semibatch solvent exchange was accomplished using a rotary evaporator with an integrated flow cart (Figure 10) which controlled all flow into and out of the evaporator. This method of distillation with strip to dryness and high turnover rate is an efficient and effective way to incorporate the solvent exchange unit operation into a continuous processing train. There are two main aspects this solvent exchange method that make it analogous to a continuous process. First, the evaporator is heated and held at a constant temperature at all times. The process materials heat up and cool down as they flow in and out. Second, frequency of volume turnovers is high, with about 20 turnovers per day. Intermittent flows of feed, solvent, distillate, and bottoms, were all fully controlled by the DCS automation system, using sequenced automated block valves, data logging balances, and pressure swing vessels on balances.

Solvent exchange distillation ran for a total of 244 h cumulative flow time for campaign 1 and 51 h cumulative flow time for campaign 2. The longest single run with no stops was 101.5 h. The unit operation was deliberately shut down on weekends, and often at the end of each working day, because it was not a process bottleneck. The unit operation was designed for ease of startup and shutdown with no startup or shutdown transition waste. It also enabled accurate and precise control of **2** concentration in toluene for feeding into continuous crystallization. Concentration of **2** in solutions flowing into

dx.doi.org/10.1021/op200362h | Org. Process Res. Dev. 2012, 16, 1017–1038

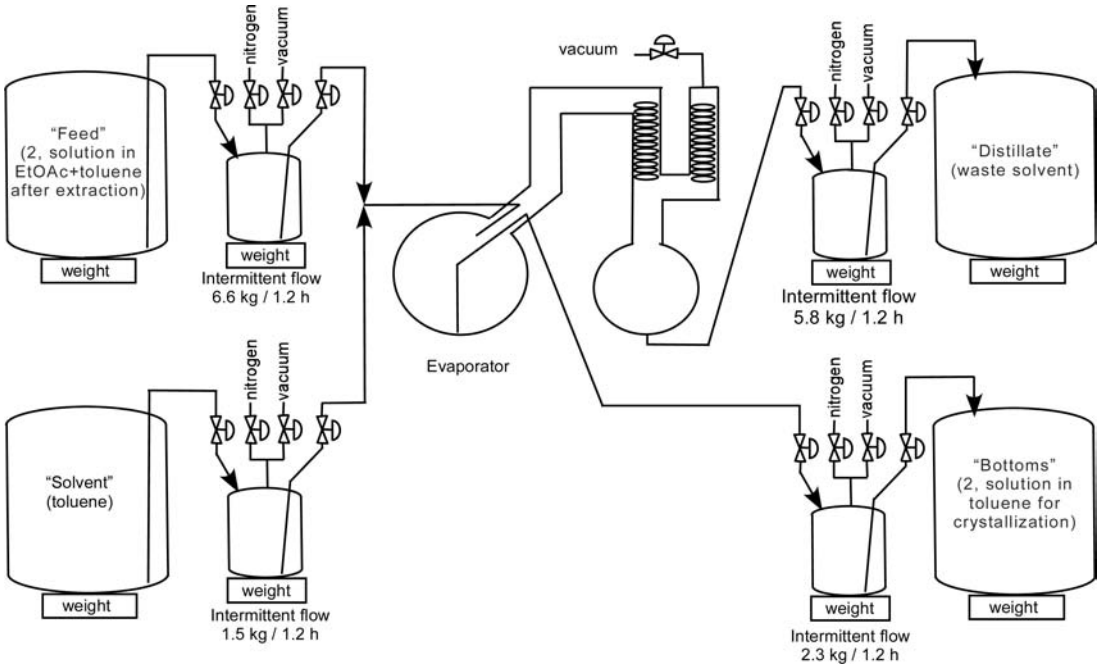

Figure 10. Flow diagram for automated repeating semibatch solvent exchange distillation with strip to dryness and high turnover rate.

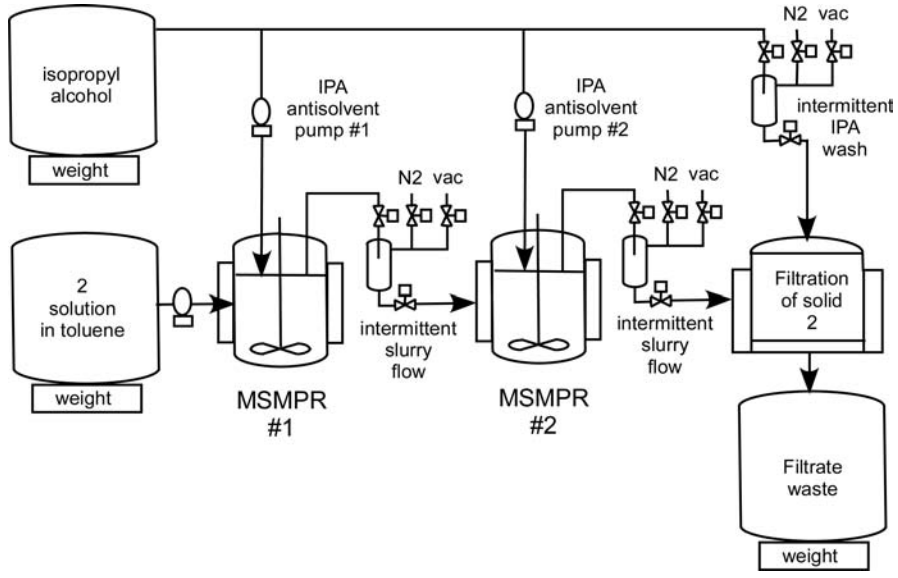

Figure 11. Equipment configuration for continuous crystallization.

solvent exchange unit operation varied by 25% over the campaign, but concentration of **2** in the solutions flowing out of only varied by 4%. This solvent exchange methodology had both throughput and environmental advantages compared to batch, and although not truly continuous it has most of the same process intensification and automation of continuous unit operations. Each 48 h of cumulative flow time, a 20 L evaporator processed about 312 L of **2** solution post extractive workup. If a batch plant process were to operate on a 48-h start to start cycle time, a 400 L batch tank would be required for the comparable solvent exchange throughput. In the batch solvent exchange process, the crude mixture is concentrated to 4 volumes total solution based on the **1** used in the reaction. This distillation is performed under reduced pressure (0.12 bar) and 40−50 °C to avoid any possible epimerization of **2** if any acid is present. After the first concentration, the solvent composition is 90% toluene and 10% ethyl acetate. Five volumes of toluene is then added and again concentrated to about 28% **2**. After the second concentration the composition is 99.7% toluene and 0.3% ethyl acetate. In comparison, the automated rotary evaporator process concentrated the crudes to dryness under vacuum and 40−50 °C, and only 3 volumes toluene was added to achieve a concentration of about 27% **2**. The concentration of ethyl acetate was less than 0.1% using this process. Thus, there was a 40% reduction in toluene compared to the optimized batch process, and residual ethyl acetate was lower. A practical throughput limit for the flow cart that was used in this campaign would be about 800 L/day feed solution at about 10% nonvolatiles, which is accomplished with three 50 L rotary

evaporators running simultaneously in parallel by the single automated flow cart.

Crystallization and Filtration. Crystallization of **2** was required to remove processing impurities and to upgrade chiral purity from about 94.5 ee to >99% ee. The crystallization was designed as an antisolvent (isopropyl alcohol) driven process from toluene. This was accomplished with a 2-stage mixed suspension mixed product removal (MSMPR) cascade and 2 single plate filters in parallel (Figure 11). The figure only shows the online filter.

The feed solution and portion of the IPA antisolvent were both continuously pumped into the first tank where a fraction of **2** continuously crystallized. The slurry from the first MSMPR crystallizer was pumped intermittently and the remaining IPA antisolvent was pumped continuously into a second MSMPR in series which continuously operated at "end of crystallization" conditions with low steady-state supersaturation. Slurry from the second MSMPR was pumped intermittently to one of two single plate filters in parallel. The solids were removed from the offline filter and dried. For research scale MSMPRs, other researchers have also used intermittent flow of slurries out of the stirred tank[17] which minimizes plugging fouling and minimizes τ in tubes and pumping mechanisms.

Continuous crystallization has been practiced in industry for several decades, as described in textbooks.[18] The two main categories of continuous crystallizers recently used for research and development in the pharmaceutical industry are tubular PFR[19] and MSMPRs.[20] MSMPRs were chosen for design and development of the antisolvent driven crystallization described in this paper. The primary goal of this crystallization was impurity rejection and chiral ee upgrade. Research scale MSMPRs are also well described in literature on crystallization of inorganic compounds.[21] The MSMPRs used in this study are similar to those described elsewhere, except that supersaturation is mainly generated by antisolvent addition rather than cooling. Antisolvent crystallization could also be done in a PFR, but several addition points would be needed in order to maintain low supersaturation at all points along the PFR.

In a MSMPR, it is known that seeding is not required at steady state because there is a steady-state birth rate of nuclei. At moderately low degrees of supersaturation, steady-state secondary nucleation may be governed by surface activation, and at lowest degrees of supersaturation secondary nucleation may be governed by attrition.[22] It has also been shown that kinetically controlled concentration of impurities incorporated into the crystals in an MSMPR can be different than impurity incorporation at thermodynamic equilibrium.[23] This concept led us to investigate whether continuous crystallization in a steady-state kinetic regime would have favorable enantiomer rejection compared to thermodynamic equilibrium. MSMPRs can be used for particle size and polymorph control, and to determine crystal growth rate and birth rate constants by measuring particles sizes at steady state, and solving population balance equations using numerical methods to fit to the measured particle size data. In addition, MSMPR cascades can be modeled to predict CSD by simultaneous solution of population balance and mass balance equations. However, in this work impurity rejection was the driver for applying MSMPR technology. The crystals are subsequently redissolved at the start of the next step in the synthetic route; crystal size control is only required for filtration. Therefore the results and discussion in this paper focus on HPLC purity results only.

The relevant crystallizations for campaign 1 are represented by sections A1 and A2, while the campaign 2 crystallization runs are represented as sections B1, B2, C1A, C1B, C1C, and C2 in Table 9. The longest continuous crystallization run without interruption was 91.5 h, ended by a planned shutdown, not due to operational issues. After the 91.5 h continuous run, all subsequent runs were in the range 46−73 h. None of these runs was terminated due to fouling, plugging, or any other operational issue. The runs were all shut down due to exhausting the feed material. Important aspects of the equipment design that enabled the process to run for long time periods without solids plugging or fouling were (1) intermittent flow slurry pumping mechanism with automated block valves and pressure swing transfer chambers, (2) design of mixing, baffling, and inlet engineering for effective blending of antisolvent with dissolved compound without back-flow into the entry tubing, and (3) operation of both MSMPRs at low relative supersaturation. It is known that MSMPRs require up to 10 mean volume turnovers (10 τ) to reach steady-state of CSD[18, 19, 20], although it is often difficult to observe measurable differences in liquid-phase concentration after five volume turnovers. Nevertheless, 10 τ = 15 h was considered the requirement for steady state in MSMPR1.

Table 9. Summary of continuous crystallization sections for campaigns 1 and 2

campaign	section	crystallization feed material	total mass **2** in feed solution (kg)	flow time (hours)	# start−stops	total mass isolated **2** (kg)
1	A1	ee = 94.7%, 0% **1**	71.9	159.4	3	59.7
	A2	ee = 94.7%, 0% **1**	71.4	164.2	2	61.8
2	B1	ee = 92.4%, 0.3% **1**	0.29	12	1	0.23
	B2	ee = 93.6%, 0.1% **1**	6.1	47.5	1	5.4
	C1A	ee = 94.7%, 0.12% **1**	7.6	48.5	1	6.7
	C1B	ee = 94.7%, 0.12% **1**	7.5	46.5	1	6.6
	C1C	ee = 94.7%, 0.12% **1**	0.28	22.3	1	0.23
	C2	ee = 94.5%, 1.87% **1**	4.2	46	1	3.7

Campaign 2 was used as an opportunity to probe the effectiveness of the crystallization with a variety of crude product compositions. Campaign 2 sections were categorized based on crystallization feed solutions. Sections C1A, C1B, C1C was the crystallization feed solution generated from baseline reaction conditions, which was highest % ee in situ and considered most representative of best process conditions. Sections B1−B2 had lower in situ % ee than normal, resulting from higher reaction temperatures used during hydrogenation. Section C2 had higher % unreacted **1** than usual because **1** was spiked into the product receiving tank downstream from continuous hydrogenation. Each section of **2** in campaign 2 was processed separately adjusting volumes and flow rates to provide run lengths of approximately 48 h for each.

Samples of product slurry from each MSMPR were manually pulled, filtered and analyzed. The ee of the solid and wt % of **2** in the sample filtrates were tracked throughout the crystal-

dx.doi.org/10.1021/op200362h | Org. Process Res. Dev. 2012, 16, 1017−1038

lization (Figures 12 and 13). These figures show results for crystallization of section C1A, which is most representative of

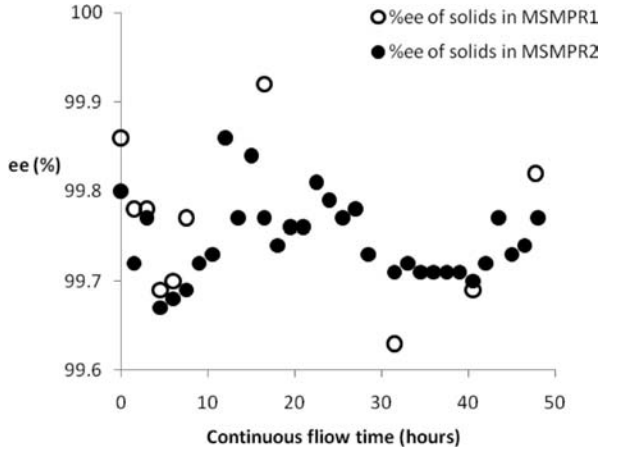

Figure 12. Baseline crystallization conditions (section C1A) % ee of solids in MSMPR1 and MSMPR2.

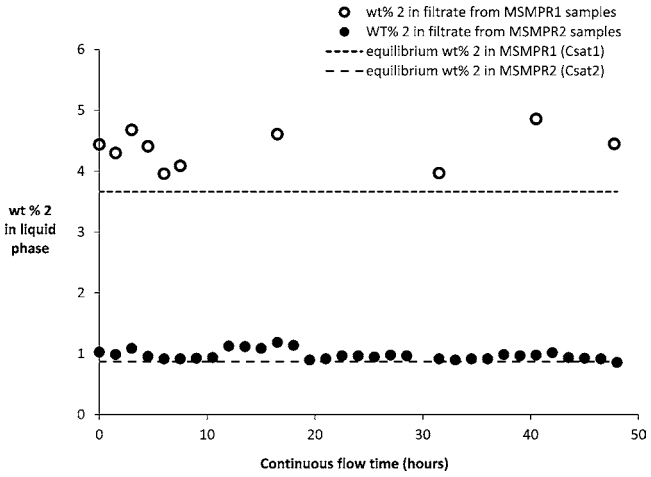

Figure 13. Baseline crystallization conditions (section C1A) wt % **2** dissolved in liquid phase in MSMPR1 and MSMPR2.

typical baseline crystallization feed. These data clearly show the consistency in ee over both MSMPRs well above the target specification of 99% ee, because minimum value for the run was >99.6%. The consistent product quality from the crystallization is one benefit of steady-state operation.

During the run after reaching steady state, slurry samples were taken from MSMPR2 in triplicate near the top and near the bottom and analyzed for percent of solids to determine whether there was any classification in the crystallizer. The results confirmed two things. First, this verified 100% uniform solids suspension mixing, which proved that agitation and baffling was sufficient. Second, it verified that wt % solids pumping out of the MSMPR was representative of wt % solids remaining; therefore, suspended solids did not accumulate in the MSMPR over time, one of the fundamental theoretical assumptions of MSMPRs.

The most significant advantage to running crystallization of **2** continuous instead of batch was the kinetically controlled vs thermodynamically controlled rejection of the undesired enantiomer. Solid-phase crystals in MSMPR2 had >99.6% ee at steady state throughout the entire 48 h run as seen in Figure 12. This is remarkable because the solid phase in the crystallizer would gradually decrease in purity from >99.6% ee down to about 95% ee if allowed to age until thermodynamic equilibrium. This is shown in Figure 14 where simply aging slurry taken out of the MSMPR resulted in ee degradation over a 20-h time period.

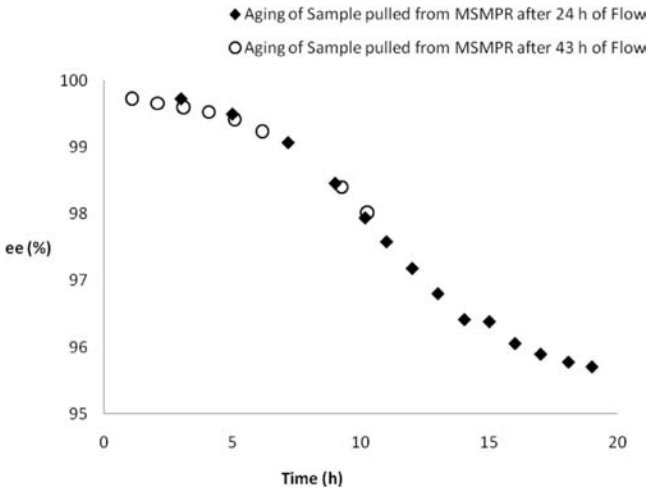

Figure 14. Erosion of product ee to thermodynamic equilibrium by batch stirring.

One 50 mL sample of slurry from MSMPR2 was removed after 24 h of continuous operation, and a second 50 mL slurry sample was removed after 43 h of continuous operation. These samples were stirred for extended periods of time at 2−5 °C. The ee of the solid decreased to near the ee of the feed solution indicating that <96% ee solid was the thermodynamic product after about 20 h. In fact, ee had dropped to lower than the target specification of 99% after the first 8 h (Figure 14). The eutectic point measured separately was 95% desired and 5% undesired enantiomer. Distribution coefficient is defined as the ratio of impurity concentration to product concentration in the solid phase, divided by that same ratio in the liquid phase. Clearly, the distribution coefficient is much lower at steady state in flow compared to batch at equilibrium.

The prospect of relying upon a metastable intermediate as a control point for chiral purity is generally considered an undesirable position, and it is not a broadly accepted impurity control strategy at Eli Lilly and Company. The risks of trending toward thermodynamic equilibrium during the continuous run are significant and require thorough investigation. However, the fact is that it provides robust and scalable impurity rejection for this crystallization. Figure 15 data support the claim that ee of the product is dominated by kinetics not thermodynamics in the MSMPRs. It shows dynamic recovery from low ee to high ee after intentionally stopping flows for about 14 h to deliberately allow the ee to decrease toward equilibrium. Flows were restarted at baseline continuous processing conditions, and ee of solids in MSMPR2 trended back up from <96% to >99.5% after just 6 τ. The experiment was done in this manner to prove that kinetic control dominated the ee of the product. Furthermore, this is an effective but controversial approach to impurity rejection, because one viewpoint is to rely solely on thermodynamic equilibrium driving forces for impurity rejection by crystallization. Nevertheless, the kinetic control of enantiomer rejection is impressive.

dx.doi.org/10.1021/op200362h | *Org. Process Res. Dev.* 2012, 16, 1017−1038

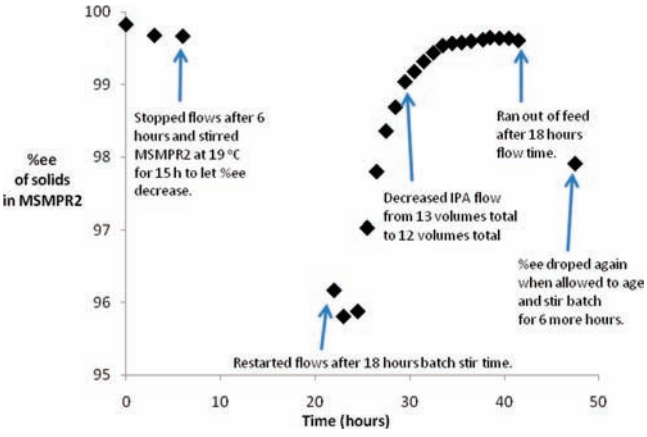

Figure 15. Percent ee of solids in MSMPR over time shows that kinetic control dominates impurity rejection.

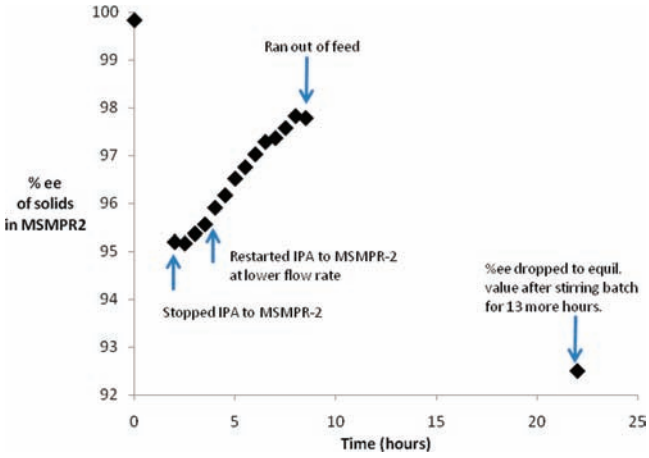

Figure 16. Percent ee of solids in MSMPR2 over time, showing that step changes in the amount of IPA antisolvent reverse the downward trend in ee.

At the end of each section during campaign 2, both MSMPRs were allowed to age to measure the concentration of **2** in the liquid phase at equilibrium. Previous runs had shown that 1 h is sufficient for desupersaturation after flows stop. This was compared to the average steady-state **2** concentration during the run. From these values, averaging over all sections of the campaign, relative supersaturation was 8% and 6% in MSMPR1 and MSMPR2, respectively. Relative supersaturation was calculated as $(C - C^*)/C^*$, where C is steady-state **2** concentration is the liquid phase and C^* is the equilibrium value at that temperature and liquid-phase composition. The calculated yield loss was 1% due to steady-state supersaturation in MSMPR2. This means that yield would be 1% higher if we allowed the crystallizers to reach thermodynamic equilibrium before filtering. Achieving >99% ee product was much more important than achieving 1% higher yield for this penultimate intermediate; therefore, the impurity rejection advantage of continuous MSMPRs outweighed the 1% yield loss disadvantage compared to that of batch.

The ee of solids in MSMPR2 could be increased dynamically by decreasing IPA flow rate to MSMPR2, all else constant. This was done to accommodate feed solutions with lower than baseline ee in crystallization sections B1 and B2. In other words, if the ee of feed solution was only 92−94%, then relative flow rate of IPA was decreased so that isolated product was still >99% ee. More importantly, if the ee dropped below 99% in the middle of a continuous crystallization run, then lowering the IPA flow rate and continuing to run would cause the ee of solids in the MSMPR to climb back up to >99% after a predictable number of volume turnovers.

Data from continuous crystallization of section B1 is shown in Figure 16. This experiment demonstrated the ability to dynamically reverse the downward trend of ee in MSMPR2 solid phase by making a step change in IPA in the middle of a continuous run. This represents a different scenario than what was shown in Figure 15, because feed flow was not stopped in this experiment. The continuous process was run using feed with 92.4% ee (section B1) vs baseline 94.7% ee. As a result, ee was rapidly decreasing after startup at baseline flow conditions, and it dropped to near 95% within the first 2 h of flow. The lower ee starting solution causes undesired enantiomer to crystallize faster. Impurity crystallization rate is proportional to concentration of impurity in the crystallizer. The flow of antisolvent to MSMPR2 was then stopped, and all other process flows continued until the amount of antisolvent present in MSMPR2 was reduced to 8 volumes total. IPA flow to MSMPR2 was then restarted at 3.2 volumes rather than the baseline 8.2 volumes. This maintained 8 volumes total in MSMPR2 rather than baseline 13 volumes, as IPA flowed continuously into MSMPR1 and MSMPR2 at 4.8 volumes and 3.2 volumes, respectively. The ee of the solid in MSMPR2 started increasing as soon as IPA flow was stopped and continued to increase when the IPA flow to MSMPR2 was restarted at 3.2 volumes. Unfortunately, the experiment was ended before reaching steady-state % ee value in the solids because the feed supply was exhausted. This process only ran for about 3 τ at desired conditions before the feed ran out, whereas 10 τ is required for CSD steady state and 6 τ is required to achieve relatively steady liquid-phase impurity concentrations. After 3 τ, ee had risen from 95% to 98% and was still climbing when feed ran out.

Rejection of starting material **1** by continuous crystallization was demonstrated with section C2 material. The feed was spiked with 1.87 area % **1** by HPLC. The continuous crystallization process provided the desired ee upgrade and rejection of **1** to a level of 0.4−0.5 area %. Interestingly, batch crystallization results in 0.32% of **1** in the crystals. In this case, impurity distribution coefficient is higher in the MSMPRs than batch and suggests that rejection of **1** could be better in a batch crystallization than continuous. It was not a problem for this particular intermediate because the acceptable level of **1** to forward process was 0.5% and because 1.87% was unrealistically high, given that typical values are <0.2% in situ after reaction. The important point is that impurity rejection is different between batch at equilibrium and MSMPR in a kinetic regime for this impurity as well.

The following figures show continuous crystallization operating performance for the entire campaign 1 (Figure 17) and campaign 2 (Figure 18), which represent a total of 512 h flow time. The 512 h flow time was cumulative over nine individual runs. The plots show % ee in MSMPR2 solids and % ee in the isolated solid after filtration and drying unit operations, for the entire 512 h flow time of the two campaigns. Vertical lines on the plots represent stops/restarts between individual sections. Stirred tanks and tubes were visually cleaned by solvent rinsing between sections.

The lower ee of samples from MSMPR2 in the first run of section A1 of campaign 1 were a result of the sampling

dx.doi.org/10.1021/op200362h | Org. Process Res. Dev. 2012, 16, 1017−1038

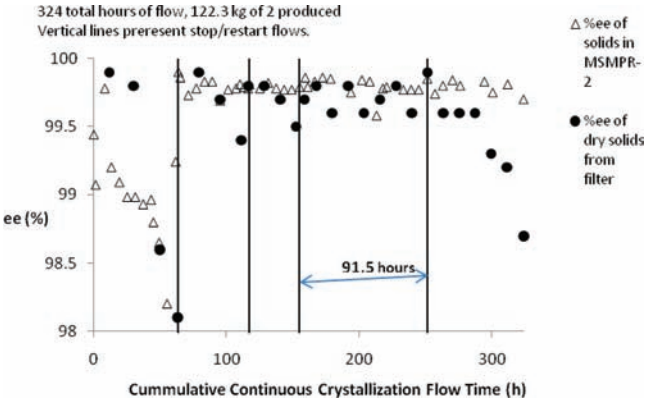

Figure 17. Campaign 1 continuous crystallization results.

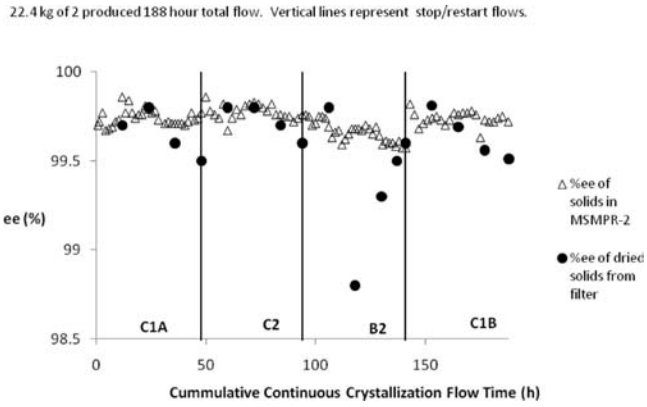

Figure 18. Campaign 2 continuous crystallization results.

technique. The slurry samples taken from MSMPR2 were filtered and the solids were submitted for analysis wet with filtrate. The filtrate contained undesired enantiomer and caused slightly lower ee results. All samples starting with the second run of section A1 were washed to remove the filtrate. The washed solids provided ee results that more accurately reflected the ee of the solid in MSMPR2.

Section C1B crystallization was run one month after section C1A crystallization to demonstrate stability of crystallization feed solution. After solvent exchange distillation, section C1 material was split in half and the second half was held in an inerted stainless steel container at room temperature for 1 month aging time. Yield and % ee of product **2** were the same for continuous crystallization and isolation of both sections.

Three main equipment configurations were used for the campaigns. The main reasons for the changes were around filter management to prevent ee degradation on the filter. These changes included pressure vs vacuum filtration, frequency and volume of intermittent slurry flow to the filter, frequency and volume of intermittent IPA wash, 2 vs 3 stirred tanks in series, and automation of the intermittent cake washing process. The first 159 h of continuous crystallization, section A1, were done with 2 MSMPRs in series that had relatively constant flow out of both crystallizers. Intermittent flow out of each was about once every 2 min. The main benefit of intermittent flow was that it allowed robust slurry pumping out of each MSMPR for long operating times without solids fouling and plugging.[24] Filter cake was not intermittently washed. Filtration was accomplished by positive pressure across the filter pad supplied by the same pumping mechanism that pushed slurry intermittently from MSMPR2 to the filter by pressurized nitrogen. As a result of the high-frequency small volume slurry slug flow to the filter, distribution of the slurry on the filter was poor as shown in Figure 19a. This is obviously an example of poor filter management. Marginal improvement was made by redirecting slurry flow entering the filter as shown in Figure 19b, but this was still poor because the filter cake did not spread out evenly and flat on the pad. After section A1 was completed, additional equipment changes and larger volume slurry drops to the filter led to much better filter cakes almost completely flat on the pad, not shown in the pictures.

The next 164 h section, section A2, was done with an additional finishing tank between MSMPR2 and the filter. Actually, 2 finishing tanks were used that operated in parallel so that slurry flow out of MSMPR2 was not interrupted. The use of alternating finishing tanks enabled intermittent flow of 10.6 L slurry to the filter once every 90 min to provide better distribution of solid on the filter, although % ee dropped between MSMPR2 and the filter (Figure 17), therefore this was still not the optimal equipment configuration. Each 90-min intermittent slurry transfer to the filter was followed by a 0.7 L IPA filter wash to prevent more impurity crystallizing out of solution on the wet cake as it awaited the next slurry drops. Vacuum in the filtrate receiver was the driving force for intermittent slurry and wash flows to the filter. Finally, the last 189 h of continuous crystallization, sections B2, C1A, C1B, and C2, used only 2 MSMPRs in series (i.e., no finishing tank), but slurry was pumped directly from MSMPR2 to the filter intermittently once every 30 min, followed by automated intermittent wash. The driving force for filtration was supplied

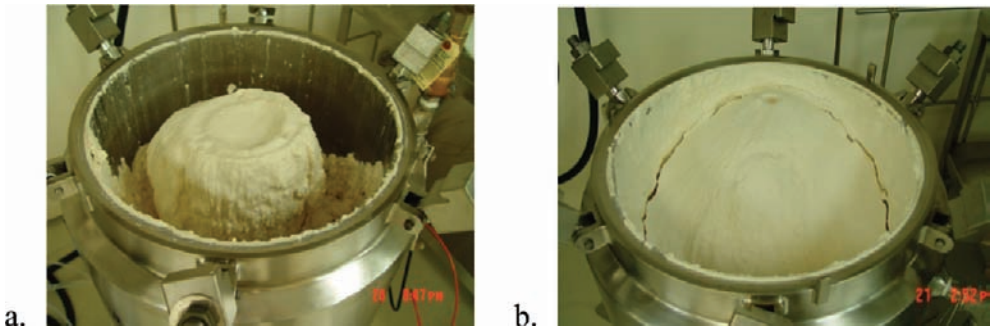

Figure 19. (a) Intermittent slurry flow to filter once every 2 min dropping vertically onto the center of the filter pad; (b) Slurry flow redirected toward the wall in the radial direction entering the filter.

dx.doi.org/10.1021/op200362h | Org. Process Res. Dev. 2012, 16, 1017–1038

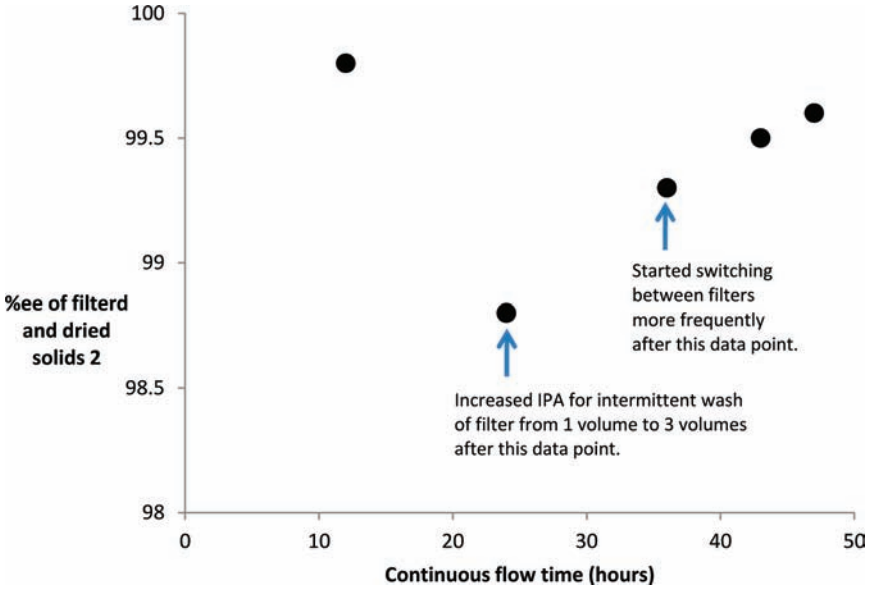

Figure 20. Percent ee of filtered and dried solids from 48 h continuous crystallization run of section B2, which started with only 93.6% ee in solution.

Table 10. Data summary for isolated 2 from campaigns 1 and 2 after drying

campaign	number of lots	average lot size (kg)	average % potency for all lots (with st dev)	average % TRS for all lots (with st dev)	average % ee for all lots (with st dev)
1	29	4.19	99.26 (0.44)	0.680 (0.067)	99.46 (0.61)
2	20	1.12	98.01 (0.59)	0.812 (0.284)	99.64 (0.25)

as positive pressure from the intermittent pumping mechanism rather than vacuum filtration.

Data gathered during the campaign 1, section A1 showed ee decreasing over time of the solid isolated from the filter and dried (Figure 17). Sampling and analysis proved that the ee of the material on the bottom of the filter decreased over time upon repeated exposure to filtrate enriched in racemate. The jacketed filter was kept cold (0−10 °C) throughout the run.

During campaign 2, sections B2, C1A, C1B, C2, % ee decrease on the filter was less. This was improved in the second half of campaign 1 (section A2) by larger slurry drops and intermittent washing of the filter cake. Other than section B2, however, final isolated solids were still all >99.5% ee. Section B2 feed solution was only 93.6% ee in solution because it resulted from the higher temperature reaction section, 90 °C. Therefore it was more susceptible to ee decline in the MSMPRs and on the filter, due to higher enantiomer concentration in solution and therefore higher driving force for its crystallization. Figure 20 shows, however, that the decreasing trend of ee on the isolated solids was reversed dynamically in the middle of the 48 h B2 run by changing the cake washing. In the figure, each data point represents one filter full of solids, accumulated over 12 h processing time for each of the first three filters, and 5−7 h processing time for each of the last 2 filters.

Increasing the size of the intermittent wash to more effectively remove the filtrate containing the enantiomer and reducing the filter collection time from 12 h to 5−7 h were step changes made in the middle of the continuous run to reverse the observed decrease in ee of isolated dried solids. The ee of the samples from the bottom of the filters following these changes showed significant improvement. This real time improvement in ee as a result of a step change in filter management in the middle of a 48 h run was additional data indicating a kinetically controlled enantiomer rejection. These results indicated filter management was critical to maintaining the high ee of isolated solids. Centrifugation with better cake de-watering and washing capabilities combined with frequent discharges would be ideally suited for this isolation.

The final results for campaigns 1 and 2 are summarized in Table 10. For campaign 1, a total of 140 kg of **1** was processed through the entire continuous sequence and 121.6 kg of **2** was obtained in 87% yield (potency corrected). The chiral purity was 99.5% ee on average, and the product contained <0.03% *trans* impurity **6** and 20 ppm rhodium. For campaign 2, a total of 26.1 kg of **1** was processed through the entire continuous sequence, and 22.4 kg of product was obtained in 84% yield (potency corrected). The chiral purity was 99.6% ee on average, and the product contained <0.03% *trans* impurity **6**. Average and standard deviations of TRS for campaign 2 were higher than for campaign 1 because four of the lots came from crystallization section C2, which had been intentionally spiked with 1.87% **1** prior to workup and isolation.

Each lot represents an individual filter. On average, each filter represented 10.4 h of continuous crystallization. These lots were kept separate through the drying step and analyzed separately for research and development purposes, to quantify effects of intentional changes in process parameters and equipment configurations. In manufacturing, however, there would be fewer lots and fewer batch release analytical tests.

In addition to kinetic control of rejection of undesired enantiomer, a second benefit of the continuous crystallization process was throughput. The process was operated at an input of 10.1 kg/day **2** isolating 8.8 kg/day compound **2,** using a 12 L MSMPR and a 22 L MSMPR. Each 48 h of flow time at these rates, 342 L of slurry flowed from MSMPR2 to the filter. In a batch plant operating with a 48 h start to start cycle time, the batch crystallization tank size would need to be at least 400 L to achieve the same throughput as the 12 L and 24 L MSMPRs. In

dx.doi.org/10.1021/op200362h | *Org. Process Res. Dev.* 2012, 16, 1017−1038

standard walk-in laboratory fume hoods, it would have been possible for us to isolate 20 kg/day compound **2** by using 30 L and 60 L stirred vessels. However, as stated earlier, the production campaign was deliberately run at lower flow rates to allow for longer times to establish steady state and test robustness/reliability at different sets of operating parameters.

A third advantage of continuous over batch crystallization was less material at risk in the crystallizers at any given point in time. Only about 6% of a "48-hour batch" is in the continuous crystallizers at any time. Therefore, the typical batch requirement for stable hold of the slurry in the crystallization vessel is a less significant constraint for continuous crystallization.

A fourth advantage was the use of significantly less seed than a batch process. Seed is only used during the batch startup of each stirred tank crystallizer. A total of 2.2 g of seed was used for crystallizing the entire 170 kg of **2** in feed solution which was a 0.0013% seed load. Seed loading is about 3 orders of magnitude higher for the batch crystallization process.

Most of the design and development work for the continuous crystallization was initially done using batch experiments. This includes screening studies for solubility, solvent/antisolvent selection and ratios, densities, desupersaturation kinetics, antisolvent addition rates, mixing rates, above surface vs subsurface addition, coaddition vs standard semibatch antisolvent addition, rejection of spiked impurities, stable hold points, and stability of feed solutions. The continuous crystallization experiments served to provide information that was not possible to achieve through batch experiments and numerical modeling, namely quantifying the kinetically controlled impurity rejection at steady-state MSMPR conditions, quantifying the buildup of solids over time in the MSMPRs especially at the inlets, and the buildup of solids over time in the piping and pumping mechanisms at the outlet of each MSMPR.

Parallel surge vessels were deliberately designed into the equipment train between feed mix tanks and continuous reaction, between reaction and continuous extraction, between extraction and solvent exchange, and between solvent exchange and crystallization. While one surge tank filled with solution from the previous unit operation, the other served to feed the next unit operation, in alternating fashion. This setup helped achieve and verify accurate, precise, and reliable mass flow rates, achieve and verify flow material balance for each unit operation, ensure material quality for forward processing from one continuous unit operation to the next, decouple the unit operations to keep process upsets localized, minimize and isolate off spec material, and simplify startup and shutdown transitions. The parallel surge tanks are placed on floor scales so that flow material balances and total material balances can be accurately calculated by change of mass of solutions in feed and product tanks over time. This provides redundancy on all mass flow measurements, because all inline mass flow meters are compared to actual mass flow in or out of the unit operation calculated from change in mass measured by the floor scales. Decoupling continuous unit operations with parallel surge vessels does not take away from the main benefits of continuous processing vs batch, and it provides additional quality assurance and quality control benefits to the process. The surge tanks were simple stainless steel vessels with no agitation and no temperature control because the contents were homogeneous solutions at room temperature; therefore, they were only a moderate portion of the total cost of the continuous processing equipment train. The benefits outweighed the disadvantages of needing more tanks, more floor space, and higher overall τ in the processing train.

Manufacturing Considerations. Throughput demonstrated for the continuous unit operations described in this report was about 13 kg/day of **2** in situ through reaction, extraction, and solvent exchange, and 10.2 kg/day in situ **2** in feed to crystallization. Laboratory production is not capable of commercial manufacturing-scale production of this intermediate. However, the four continuous unit operations could still be small enough to utilize portable skid-mounted continuous processing equipment at commercial scale. The manufacturing plant would still benefit from large (e.g. 2000 gal) stirred vessels for making up reagent feed solutions batch to feed the continuous unit operations, but the vessels in which chemical transformation or mass transfer separations/purifications take place could still be small enough to remain transportable. Since the time of this development work, our group has moved to a vertical-pipes-in-series PFR design because it is scalable to higher volumes and because it runs at a higher percentage liquid filled. A PFR with 15−20 vertical pipes in series is sufficient to achieve low axial dispersion numbers, high enough vapor liquid mass transfer and heat transfer rates for asymmetric hydrogenation reactions with 6 to 12 h τ, high pressure rating and low capital cost, and it runs continuous hydrogenation reactions 99% liquid filled. Continuous crystallization could still be done in MSMPRs, on the order of 100−200 L each. Pumping slurries without plugging and fouling is more robust at larger scales because of larger tube/pipe sizes and turbulent flow; therefore, a wider range of pumping mechanisms are viable. Of the four unit operations reported, continuous crystallization with its ee upgrade is unmatched by batch. Furthermore, only a small amount of material is at risk in the MSMPRs at any one time, which could be diverted in the event of a process upset. Centrifugation with its more frequent cake washes and discharges would be better than single plate filters. As common manufacturing asset, centrifugation would minimize potential for undesired enantiomer crystallization on the filter. Even though enantiomer rejection by steady-state control using continuous crystallization proved to be robust in this body of work, it is important to note that this is not yet a widely accepted impurity control strategy. Relying on steady-state kinetic control rather than thermodynamic equilibrium would indeed require significant convincing of various organizations. This strategy is not yet selected as part of an impurity control strategy for commercial manufacturing at Eli Lilly and Company, but the consistent and powerful results merit further development. However, if kinetic control is necessary, then continuous MSMPRs are fundamentally a better scale-up option than batch. As for high-pressure hydrogenation reaction, the same in situ yield and purity could be achieved in batch or continuous. However, the safety benefits of continuous vs batch hydrogenation are significant, and the capital cost savings are significant for a manufacturing plant that does not already have existing 70-bar hydrogenation capacity.

■ CONCLUSIONS

Continuous processing enabled pilot-scale throughputs in standard laboratory fume hoods and laboratory hydrogenation bunker. When all four continuous unit operations were running simultaneously, throughput was equivalent to what we would expect from a plant module with 400 L vessels. The two unit operations that benefitted most from continuous instead of

batch processing were reaction and crystallization. A simple and economical PFR tube was designed, demonstrated, and scaled up for homogeneously catalyzed high pressure asymmetric hydrogenation. The main reason that this reaction benefitted from continuous processing was safety. Compared to batch reaction at the same kg/week throughput, there is less hydrogen in the PFR at any one time, and maximum feed rate of hydrogen from the supply cylinders is less. Reaction time and impurity profile in the PFR was the same as reaction time and impurity profile achieved in a batch autoclave. The main reason why crystallization benefitted from continuous processing was because the kinetically controlled impurity rejection of undesired enantiomer was highly favored over thermodynamically controlled rejection. At thermodynamic equilibrium the isolated product from this process had about 95% ee as expected from the eutectic. In contrast, the isolated product from a kinetically controlled continuous crystallization had about 99.5% ee or higher. Robust kinetic control was demonstrated by deliberately stopping flows and allowing the solids in a crystallizer to trend to thermodynamic equilibrium at <96% ee, followed by restarting flows and proving that isolated product quality dynamically recovered to >99.5% ee. This is not a broadly accepted impurity control strategy but the impressive data and the consistent and repeatable results warrant consideration. Continuous extraction in mixer-settlers in series was effective for removing zinc from reaction product solution and practically eliminating the need for manual phase cuts. Automated repeating semibatch solvent exchange distillation using a rotary evaporator made strip to dryness a legitimate processing option at pilot scale, which reduced solvent waste compared to batch. It was an efficient and effective way to incorporate this unit operation into a continuous processing train, because the evaporator is heated to a constant temperature at all times, the process materials heat up and cool down as they flow in and out, and frequency of volume turnovers is high, with about 20 turnovers per day.

EXPERIMENTAL SECTION

Asymmetric Hydrogenation of Enone 1. (4-(Benzyloxy)phenyl)((1*S*,2*R*)-2-(2,5-bis(benzyloxy)phenyl)-cyclopentyl)methanone (**2**):

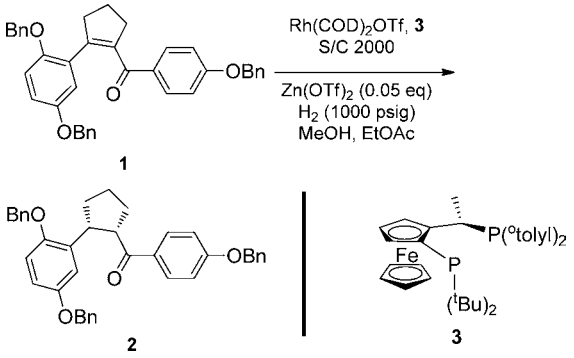

Mix Starting Material Feed Solution. To a 50 L agitated flask equipped with an overhead stirrer and a nitrogen sweep was added ethyl acetate (25.2 L), methanol (10.4 L), **1** (3.6 kg, 6.35 mol), and zinc triflate (113 g, 0.31 mol, 0.05 equiv). **1** was filtered across Sunsource filter prior to charging due to black specks noted in the first drum. The mixture was stirred under nitrogen for 15 min to dissolve all solids. This process was repeated as needed throughout the campaign duration (3 to 4 times per day). Approximate dry bulk density of 1 was 1.5 kg into 5 L. The starting material solution was transferred to one of two parallel stainless steel 200 liter feed vessels for continuous reaction. The feed vessel was sparged with nitrogen to remove oxygen before switching feed tank on line to the high pressure feed pumps. Volumetric sparging ratio was about 10 L/min per 100 kg feed solution, during which time 0.1% of the total solvent was stripped and collected in a dry ice trap in the vent line from the vessel.

Precatalyst Preparation. The metal ligand complex or "pre-catalyst" was prepared by stirring $Rh(COD)_2OTf$ and diphosphine ligand in methanol at room temperature in a drybox. The precatalyst and reduced active catalyst are extremely sensitive to oxygen in solution and can rapidly deactivate. A solution of precatalyst was prepared by combining $[Rh(COD)_2]BF_4$[1] (3.5 g, 8.62 mmol) and ligand **3** (purchased from Solvias AG, Basel, Switzerland) (5.4 g, 9.47 mmol), 1.1 equiv relative to $[Rh(COD)_2]BF_4$) in a glass pressure vessel. The solids were degassed via vacuum−nitrogen refilling and transferred into a drybox. Degassed anhydrous MeOH (500 mL) was added to the solids and stirred until dissolved. While stirring for 2 h, the catalyst solution changes color from orange to dark red. If the color changed to brown, this was an indicator that the catalyst had been exposed to oxygen and was compromised. We found that solution of precatalyst could be stored in the drybox for over 1 month without any drop in reaction performance. The precatalyst solution was transferred from the drybox to the continuous reactor feed pump in a pressurized feed bottle.

Reactor Filling (Solvent Only). The starting material feed pump was filled with degassed 30% methanol in ethyl acetate and the precatalyst feed pump was filled with degassed methanol. The gas feed was nitrogen instead of hydrogen during the solvent-only startup run, and the reactor gradually pressured up to 69 bar with the controlled nitrogen gas feed. The reactor was heated to 70 °C. The starting material, precatalyst and toluene pumps were started. Flows were continued for at least 1 reactor volume turnover (12 h) to confirm flow rates and mass balance. The gas feed was then switched to hydrogen (69 bar) and the flows were continued for at least 3 h with solvent only.

Reaction. The parallel precatalyst pump was charged with precatalyst solution from a pressurized feed bottle (see above). The source tank feeding the starting material pump was switched to the 55 gallon feed tank containing **1**/$Zn(OTf)_2$ solution. The pumps were started at feed rates targetting τ = 12 h and a S/C = 2000:1. There were three continuous feeds that mixed together at the inlet of the PFR; the catalyst solution, the solution of compound **1** and $Zn(OTf)_2$, and hydrogen gas. Toluene mixed into the reaction product solution continuously in a "T" at the outlet of the reactor. The product solution continuously flowed through a cooling and depressurization system and into one of two 200 L parallel stainless steel surge vessels. Table 11 lists flow values for the continuous reaction:

The campaign 1 reaction flowed for a total of 282 h under these conditions (not counting the one weekend flow stoppage in the middle). Shutdown was done by switching liquids back to solvent only, flowing 14 h at the same rates, the switching gas from hydrogen to nitrogen, flowing for 12 more hours to inert the system, and then stopping flows and depressurizing slowly by continuing to meter gas out the exit from the end of the reactor. There was no startup or shutdown transition waste, but the first and last sections of product solution in the surge tanks

dx.doi.org/10.1021/op200362h | Org. Process Res. Dev. 2012, 16, 1017−1038

Table 11

Flow Values	
1 feed solution flow, L/day	130.1
catalyst solution flow, L/day	0.62
toluene flow to "T" into exit of tube reactor, L/day	65.4
target hydrogen flow rate into continuous reactor, kg/day	0.086
total product solution including toluene, L/day	201.3
Calculated Flow Rates Are Based on the Following:	
equivalents hydrogen targeted for campaign	2.0
density catalyst ligand solution, g/mL	0.800
density of **1** feed solution, g/mL	0.903
density of mixture of both reaction feed solutions, g/mL	0.900
density product solution, g/mL	0.885

were slightly more dilute. (Solvent exchange compensated for this so that concentration of **2** was consistent going into crystallization.)

Although there are safety advantages of running the high pressure hydrogen reaction continuous (for example less hydrogen in the reactor at any time because the reactor is higher % liquid filled, smaller reactor for the same throughput, and lower instantaneous hydrogen flow rate from the pressure cylinders), this process is still governed by all of the typical safety considerations, precautions, and designs needed for a high pressure hydrogen explosion proof bunker. Many interlocks are in place with regards to hydrogen sensors, air turnovers in the operating area, and process pressures and temperatures. Because the reactor is a long plug flow tube, pressure relief valves were installed at both the inlet and outlet sides of the tube, set to 95 bar relief pressure. There were pressure reliefs for all positive displacement pumps, and automated shutoffs for liquid pumps and hydrogen feed system interlocked to high or low pressure readings and hydrogen gas detectors in the bunker. An additional safety benefit of continuous operation was that maximum hydrogen gas flow rate was highly restricted at the source cylinder, because instantaneous hydrogen supply rate is more than 100 times lower than for batch. In batch a large amount of hydrogen is supplied to the reactor over a short time at the beginning of the reaction, which is not the case for continuous.

All online analytical data for the hydrogenation reaction was collected using a Waters PATROL Acquity UPLC. The instrument is similar to the traditional Waters UPLC instrument in that it is equipped with a binary pumping system, tunable ultraviolet (TUV) detector (500 nL flow cell, 10 mm path length), and four-column oven with integrated column switching valves. The difference between a traditional UPLC and a PATROL is the replacement of the sample manager with a process sample manager (PSM) equipped with process, online sampling, and priming valves, diluent and sample syringe pumps, and a 2-μL fixed injection loop. The PSM utilizes a peristaltic pump to pull a sample from the reaction and to deliver it to the sampling valve, where the automated sample dilution is performed. The diluted sample is then injected onto the UPLC column.

Continuous Liquid–Liquid Extraction. Continuous extraction was done with three mixer–settlers in series. Process vessels were three pairs of 22-L glass round-bottom flasks. Temperature in each of the six flasks was 21–22 °C.

Two feeds (170.8 kg/day of reaction product solution and 66.1 kg/day of 1 N HCl solution) flowed continuously into the first mixer. Liquid level in the mixer was 11.2 L at steady state, and liquids flow continuously from the mixer to the settler. The settler flask was not agitated so that layers could separate. In the settler, the organic layer volume was 10.2 L, and the aqueous layer volume was 6.6 L at steady state. The aqueous layer flowed continuously to waste at 97.8 kg/day, while the organic layer flowed continuously to the stage 2 mixer.

Two feeds (organic solution from the first settler and 0.5 M sodium bicarbonate at 65.5 kg/day) flowed continuously into the second mixer. The liquid level in the second mixer was 10.6 L at steady state. Liquids flowed continuously from the mixer to the settler. The settler flask was not agitated so that layers separate. In the settler, the organic layer volume was 9.3 L, and aqueous layer volume was 5.0 L at steady state. The aqueous layer flowed continuously to waste at 74.1 kg/day while the organic layer flowed continuously to stage 3 mixer.

Two feeds (organic solution from the second settler, and water at 38.1 kg/day) flowed continuously into the third mixer. Liquid level in the mixer was 10.4 L at steady state. Liquids flow continuously from the mixer to the settler. The settler flask was not agitated so that layers separate. In the settler, the organic layer volume was 9.3 L, and the aqueous layer volume was 2.4 L at steady state. The aqueous layer flowed continuously to waste at 40.9 kg/day, while the organic layer flowed continuously to one of two parallel surge vessels. The product from extraction became the feed to solvent exchange distillation unit operation. All vessels were started and shut down semibatch, and proceduralized for no startup or shutdown waste.

Automated Repeating Semibatch Solvent Exchange Distillation with Strip to Dryness. The solvent exchange was done by automated repeating cycle (70 min cycle time) fully controlled by the DCS system. The operator swapped feed tanks and receiver tanks once or twice per day. Overall average flows into the system were 126 kg/day **2** solution feed, 29 kg/day toluene feed. Overall average flows out of the system were 111 kg/day distillate waste and 45 kg/day solution of **2** in toluene. The Büchi evaporator (20 L flask) bath temperature was 60 °C, and rotation was 85 rpm. All mass flows in and out were accurately controlled by DeltaV, which is a digital automation system by Emerson Process Management. DeltaV also controlled the same repeating distillation sequence. Step 1 is 165 Torr/400 s. Step 2 is 125 Torr/400 s. Step 3 is 100 Torr/400 s. Step 4 is 65 Torr/1500 s. Total time to strip to an oil was 45 min, and total discharge time before pumping out was 30 s.

The resulting solution of **2** in toluene gradually filled one of two parallel stainless steel vessels that were feed tanks to continuous crystallization. There was no startup or shutdown transition waste.

Continuous Crystallization, Filtration, Washing. The equipment configuration for crystallization of **2** was two stirred tanks in series. IPA antisolvent was split between the two MSMPRs, both operating at 2–6 °C. The process was started up as batch and then run continuous for 48 to 91 h each week before intentionally being shut down. All of the **2** slurry flowed from MSMPR1 to MSMPR2, and from MSMPR2 to the filter. All slurry flow was intermittent rather than truly continuous to achieve turbulent flow in the Teflon tube between tanks (d = 6.4 mm). This was accomplished with a pressure swing chamber and sequenced automated block valves. Filtration was done with parallel 0.41 m diameter single plate filters jacketed and cooled with glycol to 2 to 6 °C. Intermittent washing of the wet cake with IPA was also done fully automatically by the DCS system, once every 30 min immediately following a slug of

slurry flow to the filter. Average **2** concentration in filtrate + wash =0.52 wt %. Table 12lists flows and volumes for the

Table 12

wt % **2** in toluene solution	27.7
volumes IPA antisolvent to add to MSMPR1, vol	4.8
volumes IPA antisolvent to add to MSMPR2, vol	8.2
volumes IPA wash to filter total, vol	4.00
volumes IPA wash intermittent, same frequency as slurry transfer from MSMPR2 to filter, vol	3.00
volumes IPA wash final, when a filter is taken off line before discharging wet solids, vol	1.00
frequency for slurry transfer from MSMPR1 to MSMPR2, min	5.0
frequency for slurry transfer from MSMPR2 to filter, min	30.0
slurry slug size from MSMPR1 to MSMPR2, L	0.305
slurry slug size from MSMPR2 to filter, L	3.56
average τ in MSMPR1, h	1.50
average τ in MSMPR2, h	1.50
density of **2** in toluene feed solution, g/mL	0.935
density filtrate + wash, g/mL	0.798
total slurry flow from MSMPR1 to MSMPR2 estimated, L/day	87.8
total slurry flow from MSMPR2 to filter estimated, L/day	170.88
mass feed solution **2** in toluene, kg/day	36.6
IPA feed to MSMPR1, L/day	48.6
IPA feed to MSMPR2, L/day	83.1
average liquid level in MSMPR1, L	5.49
dip tube level in MSMPR1 = volume just after slurry transfers, L	5.33
2 solution to MSMPR1 at batch startup, L	2.38
total IPA to add to MSMPR1 during batch startup, L	2.96
calculated volume slurry in MSMPR1 just before slurry transfers, L	5.79
total IPA to add to MSMPR1 during batch shutdown, L	5.05
total slurry liquid level in MSMPR1 during batch shutdown, L	10.38
average liquid level in MSMPR2, L	10.68
dip tube level in MSMPR2 = volume just after slurry transfers, L	8.90
2 solution to MSMPR2 at batch startup, L	2.04
total IPA to add to MSMPR2 during batch startup, L	6.86
calculated volume slurry in MSMPR2 just before slurry transfers, L	12.46
wash IPA to filter, L/day	40.5
time between IPA wash slugs to filter, minutes	30.0
wash IPA to filter, L/slug	0.633
total filtrate + wash, L/day	202.7

continuous crystallization at most representative conditions. Both MSMPR1 and MSMPR2 were started up batch and the beginning of each continuous run and shut down batch at the end of each run, and there was no startup or shutdown transition waste. Charge amounts for batch startups are also listed in Table 12.

Batch Drying of 2. The offline filter with washed wet cake was taken into a solids containment area, the solids were scooped out of the filter and put into drying trays, and the solids were dried in vacuum ovens at 50 °C and 20 mmHg.

Synthesis of (4-(Benzyloxy)phenyl)(2-(2,5-bis-(benzyloxy)phenyl)cyclopent-1-en-1-yl)methanone (1). Reagents and Conditions: a) MsOH, 1,4-dihydroquinone (1.1 equiv), 30 °C, 36−48 h, 55% yield; b) K_2CO_3 (1.0 equiv), NaI (0.1 equiv), BnBr (1.1 equiv), acetone, reflux, 18 h, 95% yield; c) 50% aq NaOH, acetone, 65 °C, 5 h; NaI (0.1 equiv), BnBr (1.1 equiv), 50 °C, 8 h, 83% yield; d) CDMT (1.05 equiv), NMM (1.1 equiv), toluene, 0 °C, 16 h; e) 4-benzyloxyphenylmagnesium bromide (1.2 equiv), THF, 0 °C, 4 h, 90% yield over two steps.

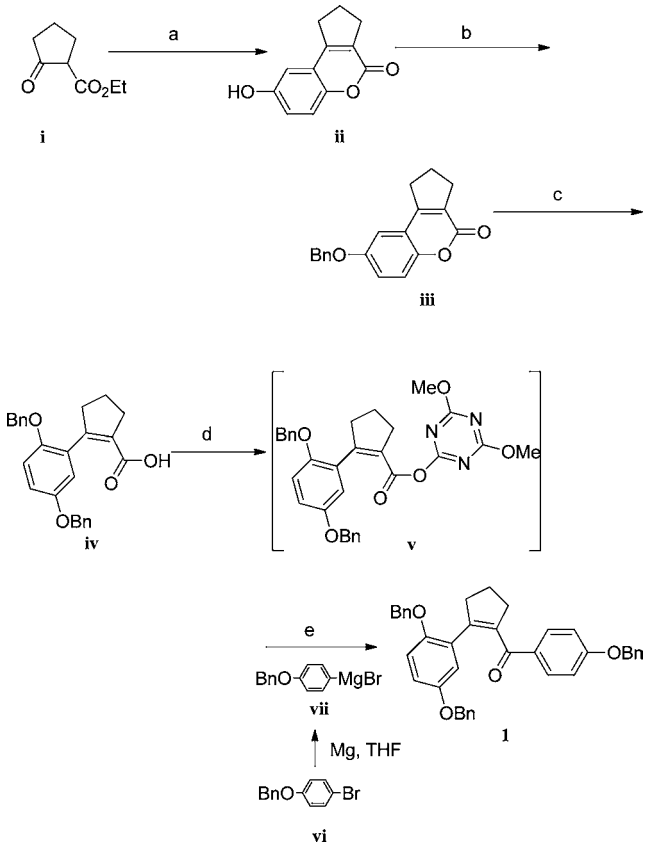

8-Hydroxy-2,3-dihydrocyclopenta[c]chromen-4(1H)-one (ii).[25] Methanesulfonic acid (708 kg) and 1,4-dihydroquinone

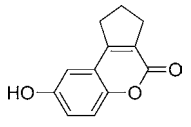

ii

(74 kg, 672 mol, 1.11 equiv) were charged into a reactor under nitrogen. The temperature was adjusted to 27−32 °C, and the mixture stirred for 1 h. To this reactor was charged **i** (94.5 kg, 605 mol, 1 equiv) over 90 min. The reaction was stirred at 27−32 °C for 45 h. HPLC analysis indicated 7.5% (wt) product with 67.5% HPLC area. Water (943 kg) was added to the reactor over 2.5 h while maintaining the temperature below70 °C. The product (**ii**) precipitated from solution during the addition of water. The temperature was gradually cooled to 15−30 °C over 4 h, and the mixture was stirred an additional 2 h. The resulting slurry of lactone **ii** was filtered. The wet cake (320.25 kg) was transferred back into a reactor along with water (373 kg). The slurry was heated to 40 °C and stirred for 4 h before an additional portion of water (619 kg) was added over 1 h. The slurry was heated back to 40 °C and stirred for 4 h. The slurry was cooled to 30 °C and filtered to afford lactone **ii** (167.95 kg, 91.6% purity, 40% assay, 55% yield corrected) as a wet cake which was used in the next step without further purification. Lactone **ii**: white solid (mp 240 °C); IR (film) ν_{max} = 3158, 2957, 2923, 1670, 1581, 1447, 1235, 1086 cm^{-1}; ^1H NMR (400 MHz, CD_3OD): δ = 9.74 (s, 1 H), 7.23 (d, J = 8.8 Hz, 1 H), 6.98 (dd, J = 8.8, 2.8 Hz, 1 H), 6.84 (d, J = 2.8 Hz, 1 H), 3.01−2.97 (m, 2 H), 2.74−2.71 (m, 2 H), 2.12−2.04 (m, 2 H); ^{13}C NMR (100 MHz, DMSO-d_6): δ = 197.4, 159.6, 156.3, 154.1, 147.3, 127.6, 119.3, 117.5, 109.9, 32.0, 30.8, 22.4; HR-

dx.doi.org/10.1021/op200362h | Org. Process Res. Dev. 2012, 16, 1017−1038

MS [ESI]: Calcd for $C_{12}H_9O_3^-$ [M − H$^-$]: 201.0557, found 201.0562.

*8-(Benzyloxy)-2,3-dihydrocyclopenta[c]chromen-4(1H)-one (**iii**).* Hydroxylactone **ii** (64.7 kg, 320 mol, 1 equiv),

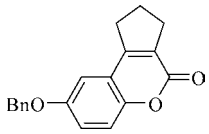

acetone (450 kg), and potassium carbonate (110 kg, 796 mol, 2.5 equiv) were added to a reactor under a nitrogen atmosphere. Sodium iodide (5 kg, 30 mol, 0.1 equiv) was added, and the reactor was heated to 22 °C over 30 min and stirred for 45 min. Benzyl bromide (61.2 kg, 358 mol, 1.12 equiv) was added, and acetone (30 kg) was used as a rinse. The reactor was heated to 55 °C for 8 h at which time HPLC analysis indicated <1% of starting hydroxylactone **ii**. The reactor was cooled 15−30 °C over 2 h. Water (325 kg) was added, and the reactor was stirred for 4 h. The resulting slurry of benzyloxylactone **iii** was centrifuged to afford 121 kg of wet cake. The wet cake **iii** was transferred back into a reactor containing acetone (360 kg). The slurry was heated to 40 °C for 4 h then cooled to 15−30 °C and filtered to afford benzyloxylactone **iii** (96.8 kg of wet cake, 99.7% purity, 93.7% assay, 97% yield corrected). The wet cake of **iii** was used directly in the next step. Benzyloxylactone **iii**: white solid (mp 188.6 °C); IR (film) ν_{max} = 3065, 2916, 1707, 1577, 1495, 1428, 1383, 1272, 1182, 1022 cm^{-1}; ^{1}H NMR (400 MHz, $CDCl_3$): δ = 7.44−7.24 (m, 6 H), 7.12 (dd, J = 8.8, 2.8 Hz, 1 H), 6.93 (d, J = 2.8 Hz, 1 H), 5.09 (s, 2 H), 3.04−3.00 (m, 2 H), 2.93−2.89 (m, 2 H), 2.23−2.17 (m, 2 H); ^{13}C NMR (100 MHz, $CDCl_3$): δ = 202.0, 160.2, 155.6, 155.0, 148.7, 136.4, 128.7, 128.2, 127.5, 119.2, 118.7, 117.7, 108.9, 70.7, 32.0, 30.7, 22.4; HR-MS [ESI]: Calcd for $C_{19}H_{16}O_3H^+$ [M + H$^+$]: 293.1172, found 293.1180.

*2-(2,5-Bis(benzyloxy)phenyl)cyclopent-1-enecarboxylic Acid (**iv**).* Acetone (221 kg) and benzyloxylactone **iii** (90.7 kg,

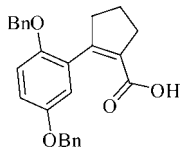

310.3 mol, 1 equiv) were charged to a reactor under nitrogen. A 10 N sodium hydroxide solution (109 kg NaOH in 280 kg water) was added to the reactor and the reaction was stirred at room temperature for 1 h. The reactor was heated to 55−57 °C and stirred for 6 h. Sodium iodide (4.41 kg, 26.6 mol, 0.1 equiv) and benzyl bromide (60 kg, 350.3 mol, 1.13 equiv) were added to the reactor along with acetone (21.4 kg) as a rinse. The reaction was stirred for 6 h at 55−58 °C. Analysis of a sample by HPLC indicated incomplete conversion and an additional portion of benzyl bromide (4.5 kg, 26.3 mol, 0.1 equiv) was added along with acetone (13 kg) as a rinse. The reaction was stirred an additional 4 h at 55−58 °C. The reaction was cooled to 30 °C and acetone (215 kg) was added followed by 6N HCl (487 kg) to adjust the pH to 1−2. The resulting slurry was cooled to 5−7 °C and stirred 4 h. The product (**iv**) was filtered to afford 121.2 kg of wet cake. The wet cake containing **iv** was charged to a reactor containing water (367 kg) where the slurry was heated to 30 °C for 4 h and filtered. The resulting wet cake containing **iv** (118.8 kg) was then reslurried a second time with acetone (220 kg) at 0 °C for 4 h and filtered. The resulting solid was dried under vacuum for 8 h to afford carboxylic acid **iv** (104.5 kg, 98.0% purity, 83.7% corrected yield) as a white solid (mp 155.9 °C); IR (film) ν_{max} = 2912, 2868, 1681, 1659, 1492, 1276, 1213, 1052 cm^{-1}; ^{1}H NMR (400 MHz, $CDCl_3$): δ = 11.9 (s, 1 H), 7.34−7.18 (m, 10 H), 6.75−6.70 (m, 3 H), 4.90 (s, 4 H), 2.75−2.69 (m, 4 H), 1.92−1.83 (m, 2 H); ^{13}C NMR (100 MHz, DMSO-d_6): δ = 197.9, 166.8, 152.5, 150.1, 149.6, 137.9, 137.7, 131.5, 129.0, 128.8, 128.7, 128.2, 128.1, 128.0, 127.6, 116.3, 114.5, 114.3, 70.8, 70.1, 34.6, 22.1; HR-MS [ESI]: Calcd for $C_{26}H_{24}O_4H^+$ [M + H$^+$]: 401.1747, found 401.1747.

*(4-(Benzyloxy)phenyl)(2-(2,5-bis(benzyloxy)phenyl)-cyclopent-1-en-1-yl)methanone (**1**).* [26]It should be noted that,

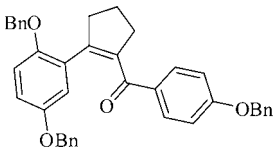

while this particular preparation of enone **1** gave good results, later campaigns experienced difficulties during processing. This highlights the sensitivity of this reaction. Grignard **vii** preparation: THF (242 kg) was added to a reactor under nitrogen. The solution was sparged with nitrogen for 90 min before bromide **vi** (76 kg, 288.83 mol, 1 equiv) was added to the reactor. In a separate reactor magnesium (8 kg, 328.68 mol, 1.14 equiv) was charged along with a portion of the solution of bromide **vi** in THF (13.3 kg). An additional 30 kg of THF was added, and the reactor was heated to 47 °C. The remaining solution of bromide **vii** (304.7 kg) was then added over 3.5 h such that the temperature was maintained between 45 and 60 °C. The reaction was stirred 11.5 h at 45−55 °C before cooling to 10−30 °C. A sample was then taken for analysis to determine concentration of Grignard reagent **vii** (0.9 mol/kg in this case). The solution of **vii** was then used directly in the next unit operation.

DMT Ester Formation. Toluene (249 kg) was charged to a reactor under nitrogen. Nitrogen was bubbled through the solvent for 1 h at 24 °C. Carboxylic acid **iv** (99.0 kg, 247.21 mol, 1 equiv), CDMT (47.5 kg, 270.55 mol, 1.09 equiv), and *N*-methylmorpholine (29.6 kg, 292.6 mol, 1.18 equiv) were added to the reactor along with degassed toluene (6 kg) as a rinse. The reaction was stirred for 16 h at which time HPLC indicated that starting material had been consumed and DMT ester **v** had formed. The slurry was filtered into a second dry reactor, and the resulting filter cake was washed with toluene (2 × 90 kg). The combined filtrates containing the DMT ester solution were cooled to −7 °C.

Coupling Reaction. To the solution of DMT ester **v** in toluene was added the THF solution of Grignard reagent **vii** (293 kg) dropwise over 5.5 h while maintaining an internal temperature between −10 and 0 °C. The reaction was stirred an additional 3.5 h between −10 and 0 °C at which time HPLC analysis indicated complete consumption of DMT ester **v**. Aqueous HCl solution (1 N, 41 kg) was added slowly over 40 min while keeping the temperature between 0 and 10 °C. Additional 1 N aqueous HCl solution (449 kg) was added slowly over 40 min while keeping the temperature between <15 °C. The mixture was stirred for 5.5 h at 10 °C before filtering away solids that had formed during the workup. The biphasic filtrate was separated, and the organic layer was washed sequentially with saturated aqueous $NaHCO_3$ solution (503 kg)

and water (495 kg). The organic phase was concentrated to 396−495 L and treated with silica gel (100 kg). The slurry was stirred for 1 h at 10−25 °C before filtering . The filter cake was transferred into a reactor and slurried with toluene (293 kg) for 30 min and filtered. The combined filtrate were concentrated under reduced pressure (T < 50 °C) to 198 L. The temperature was reduced to 30 °C, and ethanol (439 kg) was added to the reactor. Additional portions of toluene (40.5 kg) and ethanol (235 kg) were added to obtain the appropriate solvent ratio by GC. The solution (at 30 °C) was seeded with **1** (1 kg) and the temperature was adjusted to 20 °C. The slurry was stirred for 24 h before heptanes (620 kg) was added dropwise to the product slurry. The temperature was reduced to 5 °C, and the slurry was stirred for 8 h. The slurry was filtered and washed with cold toluene/ethanol/heptanes, and the resulting wet cake was dried at 40−45 °C under reduced pressure to afford **1** (107.3 kg, 97.2% HPLC purity, 96.3% assay, 74% corrected yield). **1**: white solid (mp 77 °C); IR (film) ν_{max} = 3031, 2909, 2864, 1637, 1599, 1492, 1454, 1272, 1242, 1172, 1015 cm^{-1}; ^1H NMR (300 MHz, $CDCl_3$): δ = 7.70−7.58 (m, 2 H), 7.48−7.20 (m, 15 H), 6.74−6.50 (m, 5 H), 4.99 (s, 2 H), 4.91 (s, 2 H), 4.80 (s, 2 H), 3.20−2.80 (m, 4 H), 2.19−1.96 (m, 2 H); ^{13}C NMR (100 MHz, $CDCl_3$): δ = 195.6, 161.8, 152.4, 149.9, 146.1, 139.1, 137.4, 137.1, 136.4, 131.3, 130.7, 128.6, 128.5, 128.4, 128.1, 127.8, 127.7, 127.6, 127.4, 126.9, 116.7, 115.2, 113.8, 113.2, 70.6, 70.5, 69.9, 38.9, 36.3, 22.9; HR-MS [ESI]: Calcd for $C_{39}H_{34}O_4H^+$ [M + H^+]: 567.2530, found 567.2541.

AUTHOR INFORMATION

Corresponding Author

*Johnson_Martin_D@Lilly.com; May_Scott_A@Lilly.com

Present Addresses

[⊥]Dow Corning Corporation, Midland, MI 48686.

[∥]D&M Continuous Solutions, Greenwood, IN 46143.

Notes

The authors declare no competing financial interest.

ACKNOWLEDGMENTS

The authors thank Stephen Byron Jeffery of the Eli Lilly S.A. − Irish Branch. Stephen designed the continuous reaction and crystallization process for this step that was intended for scale-up to GMP processing at Kinsale, and in doing so he guided the selection of experimental parameters and data collection for Campaign 2. We thank Todd Maloney for the on-line UPLC measurements at the exit of the hydrogenation reactor, and Gordon Lambertus and Adam McFarland for the Raman on-line probe analyses used to characterize axial dispersion in the reactor. We thank Richard Spencer, Timothy Braden, Derek Griffin, Mike Heller, John Howell, Rick Miller, Jeff Lewis, Joe Phillips, Carl Waddington, Val Hill, Bob Forbes, Brad Held, Sean Lapekas, Jeff Niemeier, and Eoin McManus for their technical contributions to the scaled up campaigns. The authors thank Ed Deweese and Paul Milenbaugh of D&M Continuous Solutions for constructing and operating the continuous processing equipment used in these internal campaigns, and Ed Plocharczyk, Shon Pulley, Jonathan Alder, Doug McKinney, Rick Spears, Tom Martin, and Ed Chow of D&M for their technical contributions. We thank the two reviewers for their improvements to this manuscript. Finally, we thank Bret Huff for initiating and sponsoring the flow chemistry efforts in development at Eli Lilly and Company.

REFERENCES

(1) (a) Malet-Sanz, L.; Susanne, F. *J. Med. Chem.* **2012**, DOI: 10.1021/jm2006029. (b) LaPorte, T. L.; Wang, C. *Curr. Opin. Drug Discovery Dev.* **2007**, *10*, 738. (c) Wegner, J; Ceylan, S; Kirschning, A. *Adv. Synth. Catal.* **2012**, *354*, 17−57. (d) Mullin, R. Novartis and MIT Study Drug Production. *Chem. Eng. News* **2007**, *81* (41), 10. (e) Pellek, A.; Van Arnum, P. *Pharm. Technol* **2008**, *9* (3), 52−58.

(2) Calvin, J. R.; Frederick, M. O.; Laird, D. L. T.; Remacle, J. R.; May, S. A. *Org. Lett.* **2012**, *14*, 1038.

(3) Cui, X.; Burgess, K. *Chem. Rev.* **2005**, *105*, 3272.

(4) (a) Roseblade, S. J.; Pfaltz, A. *Acc. Chem. Res.* **2007**, *40*, 1402. (b) Lu, S. M.; Bolm, C. *Angew. Chem., Int. Ed.* **2008**, *47*, 8920. (c) Lu, S. M.; Bolm, C. *Chem.—Eur. J.* **2008**, *14*, 7513. (d) Lu, W. J.; Chen, Y. W.; Hou, X. L. *Angew. Chem., Int. Ed.* **2008**, *47*, 10133. (e) Saudan, L. A. *Acc. Chem. Res.* **2007**, *40*, 1309.

(5) See Experimental Section for preparation of **1** at multikilogram scale.

(6) de Bellefon, C.; Pestre, N.; Lamouille, T.; Grenouillet, P.; Hessel, V. *Adv. Synth. Catal.* **2003**, *345*, 190.

(7) de Bellefon, C.; Lamouille, T.; Pestre, N.; Bornette, F.; Pennemann, H.; Neumann, F.; Hessel, V. *Catal. Today* **2005**, *110*, 179.

(8) Stephenson, P; Licence, P.; Ross, S. K.; Poliakoff, M. *Green Chem.* **2004**, *6*, 521−523.

(9) Kunzle, N.; Soler, J. W.; Baiker, A. *Catal. Today* **2003**, *79−80*, 503−509.

(10) Günther, A.; Jhunjhunwala, M.; Thalmann, M.; Schmidt, M. A.; Jensen, K. F. *Langmuir* **2005**, *4*, 1547−1555.

(11) Bretherton, F. P. *J. Fluid Mech.* **1960**, *10*, 166−188.

(12) Constructed by D&M Continuous Solutions, Greenwood, IN.

(13) Walter, J. Weber, J.; DiGiano, F. A., Eds. *Process Dynamics in Environmental Systems*; John Wiley and Sons, Inc.: New York, NY, 1996.

(14) May, S. A.; Johnson, M. D.; Braden, T. M.; Calvin, J. R.; Haeberle, B. D.; Jines, A. R.; Miller, R. D.; Plocharczyk, E; Rener, G. A.; Richey, R. N.; Schmid, C. R.; Vaid, R. K.; Yu, H. *Org. Process Res. Dev.* **2012**, *16*, 561−562.

(15) Trachsel, F.; Günther, A.; Khan, Saif; Jensen, K. F. *Chem. Eng. Sci.* **2005**, *60*, 5729−5737.

(16) Treybal, R. E. *Mass-Transfer Operations*; McGraw-Hill: New-York, 1980.

(17) (a) Asakuma, Y.; Tetahima, T.; Maeda, K.; Hideo, M.; Fukeu, D. *Powder Technol.* **2007**, *171*, 75. (b) Miki, H.; Terashima, T.; Asakuma, Y.; Maeda, K.; Fukui, K. *Sep. Purif. Technol.* **2005**, *43*, 71. (c) Wegner, J; Ceylan, S.; Kirschning, A. *Adv. Synth. Catal.* **2012**, *354*, 17−57.

(18) (a) Myerson, A. S. *Handbook of Industrial Crystallizations*; Butterworth-Heinemann: Boston, 2002. (b) Randolph, A. D.; Larson, M. A. *Theory of Particulate Processes: Analysis and Techniques of Continuous Crystallization*; 2nd ed.; Academic Press: Toronto, Canada, 1988. (c) Mullin, J. W. *Crystallization*, 4th ed.; Butterworth-Heinemann: Woburn, MA, 2001. (d) Jones, A. G. *Crystallization Process Systems*; Butterworth-Heinemann: Woburn, MA, 2002.

(19) (a) Eder, R. J. P.; Radl, S; Schmitt, E; Innerhofer, S.; Maier, M.; Gruber-Woelfler, H.; Khinast, J. G. *Cryst. Growth Des.* **2010**, *10*, 2247−2257. (b) Alvarez, A; Myerson, A. S. *Cryst. Growth Des.* **2010**, *10*, 2219−2228. (c) Lawton, S.; Steele, G.; Shering, P.; Zhao, L. H.; Laird, I.; Ni, X. W. *Org. Process Res. Dev.* **2009**, *13* (6), 1357−1363.

(20) (a) Alvarez, A.; Singh, A.; Myerson, A. S. *Cryst. Growth Des.* **2011**, *11*, 4392−4400. (b) Kougoulos, E.; Jones, A. G.; Wood-Kaczmar, M. W. *J. Cryst. Growth* **2005**, *273*, 520. (c) Kougoulos, E; Jones, A. G.; Jennings, K. H.; Wood-Kaczmar, M. W. *J. Cryst. Growth* **2005**, *273*, 529−534. (d) Van Alsten, J. G.; Reeder, L. M.; Stanchina, C. L.; Knoechel, D. J. *Org. Process Res. Dev.* **2008**, *12*, 989. (e) Chen, J.; Sarma, B; Evans, J. M. B.; Myerson, A. S. *Cryst. Growth Des.* **2011**, *11*, 887−895.

(21) (a) Asakuma, Y.; Tetahima, T.; Maeda, K.; Hideo, M.; Fukeu, D. *Powder Technol.* **2007**, *171*, 75. (b) Miki, H.; Fukunaga, R.; Asakuma, Y.; Maeda, K.; Fukui, K. *Sep. Purif. Technol.* **2005**, *43*, 77−83. (c) Miki, H.; Terashima, T.; Asakuma, Y.; Maeda, K.; Fukui, K. *Sep. Purif.*

Technol. **2005**, *43*, 71. (d) Rauls, M.; Bartosch, K.; Kind, M.; Kuch, S.; Lacmann, R.; Mersmann, A. *J. Cryst. Growth* **2000**, *213*, 116. (e) Chan, V. A.; Ang, H. M. *J. Cryst. Growth* **1996**, *166*, 1009−1014. (f) Tanrikulu, S. U.; Eroglu, I.; Bulutcu, A. N.; Ozkar, S. *J. Cryst. Growth* **2000**, *208*, 533−540.

(22) Rauls, M.; Bartosch, K.; Kind, M.; Kuch, S.; Lacmann, R.; Mersmann, A. *J. Cryst. Growth* **2000**, *213*, 116.

(23) Miki, H.; Fukunaga, R.; Asakuma, Y.; Maeda, K.; Fukui, K. *Sep. Purif. Technol.* **2005**, *43*, 77−83.

(24) Braden, T. M.; Gonzalez, M. A.; Jines, A. R.; Johnson, M. D.; Sun, W. M. Pat. Appl. WO/2009/023515 A2, 2009.

(25) Richardson, T. I.; Norman, B. H.; Lugar, C. W.; Jones, S. A.; Wang, Y.; Durbin, J. D.; Krishnan, V.; Dodge, J. A. *Bioorg. Med. Chem. Lett.* **2007**, *17*, 3570.

(26) It should be noted that, while this particular preparation of enone **1** gave good results, later campaigns experienced difficulties during processing and lower yields. This highlights the sensitivity of this reaction.